Bayesian model reveals latent atrophy factors with dissociable cognitive trajectories in Alzheimer's disease

Supporting Information

This supplemental material is divided into **Supplemental Results**, **Supplemental Methods**, **Supplemental Figures and Tables**, and **Complete List of ADNI Investigators and Participating Institutions.**

Supplemental Results

Similar Atrophy Factors Were Obtained from Aβ+ MCI Participants

We confirmed that atrophy patterns estimated with our LDA approach would be similar during the nondemented stage compared to the resulting factors from the AD dementia group. Given the small number of the Aβ+ CN participants, we estimated atrophy factors with the 147 Aβ+ MCI participants (Fig. S3C) and confirmed that the obtained atrophy factors were highly similar, with an average correlation across all pairwise comparisons of r = 0.77. Therefore, the atrophy factors from the AD dementia patients were utilized for subsequent analyses.

Atrophy Factors Were Robust to Choice of Software

Table S1 lists the anatomical structures associated with each factor based on overlap between the atrophy maps and anatomical structures in MNI152 space as defined by FreeSurfer [1] (see **Supplemental Methods**). The volumes of individual anatomical structures in all AD dementia patients were computed using FreeSurfer. Regression analyses confirmed that volumes of anatomical structures associated with an atrophy factor were lower (after controlling for intracranial volume) in participants with higher loading on the factor (see **Supplemental Methods**). For example, the temporal factor was associated with the most severe atrophy in the structures listed by Table S1A compared with the subcortical factor ($p = 2e\text{-}15$) and cortical factor ($p = 4e\text{-}15$), whereas there were no differences between the subcortical and cortical factors ($p = 0.84$). Results for the subcortical and cortical factors are in the captions of Tables S1B and S1C. The

agreement between FSL-VBM [2] and this posthoc analysis with FreeSurfer suggested that the factors were unlikely the results of segmentation or registration artifacts.

Baseline and Longitudinal Decline of Memory and Executive Function Were Consistent Across Factor Hierarchy

The behavioral (memory and executive function) analyses were repeated for two and four atrophy factors (Figs. S6 and S8). The results were consistent with the hierarchy of atrophy factors.

For example, the temporal and subcortical factors in the three-factor model were merged as a single temporal+subcortical factor in the two-factor model. Since the cortical factor was associated with the fastest longitudinal memory decline among the three factors in the AD dementia cohort (Fig. 7A), we expected the cortical factor to be associated with faster memory decline than the temporal+subcortical factor in the two-factor model, which was indeed the case ($p = 2e\text{-}6$; Fig. S6A2).

On the other hand, the three-factor analysis of AD dementia patients suggested that the temporal factor was associated with worse memory than the cortical factor, while the cortical factor was associated with slightly worse memory than the subcortical factor (Fig. 6A). Therefore, we expected difference in baseline memory between the temporal+subcortical and cortical factors (in the two-factor model) to be diluted by the fusion of the temporal and subcortical factors, which was indeed the case ($p = 0.17$; Fig. S6A1). Therefore, additional insights into factor differences could be obtained by going from two factors to three factors.

As the number of factors was increased from three to four, the cortical factor split into frontal and posterior cortical factors. There was again consistency when comparing the four-factor results with the three-factor results. The two factors were mostly associated with similar behavioral trajectories, except that among Aβ+ MCI participants, the posterior cortical factor was associated with faster memory ($p = 8e\text{-}3$) and executive function ($p = 9e\text{-}8$) decline rates than the frontal cortical factor (Fig. S8).

As the number of factors increased, the effective (average) number of participants per factor decreased (e.g., the effective number of Aβ+ CN participants "assigned to the temporal factor" is only 5.7 for the four-factor model), thus reducing our confidence in

larger number of factors despite the successful behavioral dissociation. Therefore, this work focused on interpreting the results of the three-factor model. As the ADNI database continues to grow, future work might re-visit the question of larger number of atrophy factors.

Schematics of Memory and Executive Function Trajectories Based on Statistical Test Results

The behavioral results (Figs. 5, 6 and 7) are summarized by the schematics of trajectories in Fig. 8, which were drawn based on how memory (or executive function) of each factor declined across disease stages and how the factors compared with each other in terms of memory (or executive function) decline at each stage.

All salient features of the trajectories reflect the results of statistical tests (Figs. 5, 6 and 7). For example, the executive function trajectories of all three atrophy factors were almost flat and did not diverge at the CN stage (Fig. 8B). This was based on the fact that there was no change in ADNI-EF [3] performance between Aβ+ CN and MCI participants for all three factors (Fig. 5B1), as well as no difference in ADNI-EF decline rates between factors among Aβ+ CN participants (Fig. 7B). From the MCI stage onwards, the trajectory of the cortical factor (red curve) became increasingly steep, reflecting the test results that executive function decline of the cortical factor accelerated from CN to MCI to AD (Fig. 5B2). This was also consistent with the ADNI-EF decrease between MCI and AD (Fig. 5B1). In contrast, trajectories of the temporal and subcortical factors (blue and green curves) remained almost flat from MCI to AD because there was no difference in ADNI-EF performance between MCI and AD for the two factors (Fig. S5B1). In addition, cross-sectional and longitudinal differences between the factors (Figs. 6B and 7B) were also respected in Fig. 8B, e.g., the cortical factor was associated with the worst baseline ADNI-EF and the most rapid decline among AD dementia patients.

One salient feature of the memory trajectories was the crossing of the subcortical and cortical factors (blue and red curves), supported by the following behavioral tests. Among Aβ+ CN participants, both the temporal and subcortical factors exhibited significant memory decline rates, but not the cortical factor (Fig. 5A2). The temporal and subcortical factors showed faster memory decline than the cortical factor (Fig. 7A). These

results implied that the cortical (red) curve should be above the subcortical (blue) and temporal (green) curves immediately after CN (Fig. 8A). Among Aβ+ MCI participants, the temporal factor was associated with worse memory than the subcortical factor, but not the cortical factor (Fig. S7A1). This implies that the cortical (red) curve should be lower than the subcortical (blue) curve, closer to the temporal (green) curve. This is also consistent with the statistical test showing a significant decrease in memory performance between MCI and CN for the cortical and temporal factors, but not for the subcortical factor (Fig. 5A1). Together, the results imply that the cortical (red) curve, originally higher than the subcortical (blue) curve at the CN stage, later crossed the subcortical (blue) curve before the MCI stage.

Supplemental Methods

Quality Control for Voxel-Based Morphometry. The outputs of each VBM step were visually checked by authors XZ and NS. In practice, all the VBM steps (except for brain extraction) did not require any manual interventions. The brain extraction (FSL BET [4]) sometimes resulted in inaccurate brain extraction, e.g., part of the neck was sometimes included as part of the brain. For these problematic cases, the parameters were manually tuned until the results were satisfactory. The 810 baseline scans and 560 follow-up scans (see the second paragraph of **II. Examining Factor Robustness and Characteristics of Factor Compositions**) were processed jointly to avoid bias introduced by processing the baseline and follow-up scans separately as two independent sets. Specifically, the 810 baseline scans and 560 follow-up scans were mixed together and randomly divided into two sets, such that each set contained both baseline and follow-up scans. XZ and NS each processed one set. To ensure common quality control standards, XZ and NS independently processed a small number of the participants, compared their conclusions, and eventually reached consensus.

Quantifying the Nested Hierarchy of Atrophy Factors. An important model parameter is the number of latent factors K. Therefore, we determined how factor estimation changed from K = 2 to 10 factors. An exhaustive search was performed to quantify the possibility that two atrophy patterns in the (K+1)-factor model were subdivisions of a pattern in the K-factor model (while the remaining K-1 atrophy patterns remained similar across both models). This quantification is based on the following idea: suppose an atrophy pattern in the K-factor model divides into the i-th and j-th patterns in the (K+1)-factor model, then the average of the i-th and j-th patterns should be similar to the original pattern. To quantify the presence of this phenomenon, the Pr(Voxel | Factor) of the i-th and j-th latent factors were averaged into a single Pr(Voxel | Factor). The resulting K factors of the (K+1)-factor model were matched to the K-factor model by reordering the factors (using the Hungarian matching algorithm) to maximize the correlation of Pr(Voxel | Factor) between corresponding pairs of factors. After obtaining the optimal correspondence, the pairwise correlations were averaged across all pairs of factors, resulting in an average correlation value indicating the quality of the split (with

higher correlation values indicating a better split). By performing an exhaustive search over all pairs of i and j, we found the atrophy factor of the K-factor model whose split best approximated the (K+1)-factor model (Fig. S2A). This procedure was independently repeated using Pr(Factor | Patient) (Fig. S2B).

Cross-Pipeline Validation of Atrophy Patterns. To ensure the atrophy factors were robust to choice of VBM software (FSL [2]), we performed posthoc analyses using FreeSurfer. Recall from **Top Anatomical Structures Associated with Each Factor**, that we have assigned each MNI GM anatomical structure to each of the three atrophy factors (Table S1). The structural MRI data of the 378 (= 43 CN + 147 MCI + 188 AD) participants were preprocessed using FreeSurfer so as to obtain volume estimates of all the anatomical structures for each participant. We then verified using GLM that each factor had a smaller total volume of its assigned GM anatomical structures than the other two factors (while controlling for ICV).

For example, Table S1A shows the top GM anatomical structures associated with the temporal factor. A GLM was set up where the response variable y was the total volume of the anatomical structures listed in Table S1A, while the explanatory variables included the subcortical factor probability s, cortical factor probability c, and ICV i. Hence, the GLM was $y = \beta_0 + \beta_s \cdot s + \beta_c \cdot c + \beta_i \cdot i + \varepsilon$, where β's are the regression coefficients, and ε is the residual. The temporal factor probability t was implicitly modeled because $t + s + c = 1$. Intuitively, β_0 reflected the temporal factor's total GM volume of the structures while discounting ICV, β_s reflected the response difference between the subcortical and temporal factors, and β_c reflected the response difference between the cortical and temporal factors.

Statistical tests of whether total GM volume y varied across factors involved null hypotheses of the form $H\beta = 0$, where $\beta = [\beta_0, \beta_s, \beta_c, \beta_i]^T$, and H is the linear contrast [5]. By specifying different H's, we were able to compare different pairs of factors. For example, H = [0, 1, 0, 0] tested possible differences between the subcortical and temporal factors, and H = [0, -1, 1, 0] compared the cortical and subcortical factors.

The GLM and statistical tests were repeated using Table S1B (top GM anatomical structures associated with the subcortical factor) and Table S1C (top GM anatomical structures associated with the cortical factor).

Linear Mixed-Effects Modeling of Longitudinal Cognition Decline Among Aβ+ CN, Aβ+ MCI and AD Dementia Participants. To analyze variations in cognitive decline rates across atrophy factors, one could first estimate the decline rate for each participant and then model the estimated decline rates using GLM. However, this approach is suboptimal because participants with one or even two time points may have to be discarded because the decline rate cannot be estimated with confidence (e.g., [6]).

Here we considered the linear mixed-effects (LME) model that provides significantly improved exploitation of longitudinal measurements [7] by accounting for both intra-individual measurement correlations and inter-individual variability. Under this framework, the longitudinal cognitive decline rates can be easily compared across atrophy factors for the 188 AD dementia patients, 147 Aβ+ MCI participants, and 43 Aβ+ CN participants.

A single LME model was utilized to examine longitudinal changes in memory (ADNI-Mem [8]) across the atrophy factors in the 43 Aβ+ CN, 147 Aβ+ MCI, and 188 AD dementia patients. The same model was estimated for K = 2, 3 and 4 factors, as well as for executive function (ADNI-EF) and MMSE.

For ease of explanation, we will focus on explaining the LME model for the case of three atrophy factors and ADNI-Mem. Response variable y of the LME model consisted of the 378 (= 43 CN + 147 MCI + 188 AD) participants' longitudinal ADNI-Mem. Explanatory fixed-effects variables included binary MCI group indicator m, binary AD group indicator d, subcortical factor probability s, cortical factor probability c, interactions between group indicators and factor probabilities (i.e., $m \cdot s$, $m \cdot c$, $d \cdot s$ and $d \cdot c$), time from baseline t, interactions between group indicators and time from baseline (i.e., $m \cdot t$ and $d \cdot t$), interactions between factor probabilities and time from baseline (i.e., $s \cdot t$ and $c \cdot t$), and interactions among group indicators, factor probabilities and time from baseline (i.e., $m \cdot s \cdot t$, $m \cdot c \cdot t$, $d \cdot s \cdot t$ and $d \cdot c \cdot t$), while nuisance variables consisted of baseline age x_1, sex x_2, education x_3 and total atrophy x_4.

The resulting LME model was $y = (\beta_0 + \beta_m \cdot m + \beta_d \cdot d + \beta_s \cdot s + \beta_c \cdot c + \beta_{ms} \cdot m \cdot s + \beta_{mc} \cdot m \cdot c + \beta_{ds} \cdot d \cdot s + \beta_{dc} \cdot d \cdot c + \beta_1 \cdot x_1 + \beta_2 \cdot x_2 + \beta_3 \cdot x_3 + \beta_4 \cdot x_4 + b) + (\beta_{t0} + \beta_{tm} \cdot m + \beta_{td} \cdot d + \beta_{ts} \cdot s + \beta_{tc} \cdot c + \beta_{tms} \cdot m \cdot s + \beta_{tmc} \cdot m \cdot c + \beta_{tds} \cdot d \cdot s + \beta_{tdc} \cdot d \cdot c) \cdot t + \varepsilon$, where β's are the regression coefficients, b is the random intercept, and ε is the residual. For the same reasons provided in the previous section, the temporal factor probability and binary CN group indicator were implicitly modeled. Intuitively, β_{t0} reflected the temporal factor's decline rate at the CN stage, $\beta_{t0} + \beta_{tm}$ reflected the temporal factor's decline rate at the MCI stage, and $\beta_{t0} + \beta_{tm} + \beta_{ts} + \beta_{tms}$ reflected the subcortical factor's decline rate at the MCI stage. With this model setup, variations in age, sex, education and total atrophy were controlled for across participants.

Statistical tests were performed in two stages. First, we tested whether ADNI-Mem decline rate accelerated, decelerated or stayed the same across disease stages for each factor. More specifically, for each factor, we first tested whether decline in memory and executive function was significant at the CN stage and then examined possible changes in decline rates from CN to MCI as well as from MCI to AD. For example, to test whether ADNI-Mem decline was significant at the CN stage for the subcortical factor, the null hypothesis was $\beta_{t0} + \beta_{ts} = 0$. To test whether the decline rate changed from CN to MCI for the subcortical factor, the null hypothesis was $\beta_{tm} + \beta_{tms} = 0$. Finally, null hypothesis $\beta_{td} + \beta_{tds} - \beta_{tm} - \beta_{tms} = 0$ tested whether the decline accelerated from MCI to AD. The test results for memory and executive function are shown in Figs. 5A2 and 5B2, respectively. Details on hypothesis testing in the LME model can be found in [7].

To foreshadow the results, the hypothesis tests in the previous paragraph hinted at differences in ADNI-Mem decline rates across the factors. Therefore, statistical tests of whether ADNI-mem decline rates varied across factors at each disease stage were performed. More specifically, at each disease stage, we first performed an omnibus statistical test on whether there were differences in memory decline rates across factors and then tested for pairwise differences. Take the MCI stage as an example. Rejecting the null hypothesis $\beta_{ts} + \beta_{tms} = \beta_{tc} + \beta_{tmc} = 0$ would imply differences in ADNI-Mem decline rates across the three factors among Aβ+ MCI participants. Rejecting the null hypothesis that $\beta_{ts} + \beta_{tms} = 0$ would suggest that the subcortical factor and temporal factor were associated with different ADNI-Mem decline rates. Rejecting the null hypothesis that β_{tc}

$+ \beta_{tmc} = 0$ would suggest that the cortical factor and temporal factor were associated with different ADNI-Mem decline rates. Finally, rejecting the null hypothesis that $\beta_{ts} + \beta_{tms} = \beta_{tc} + \beta_{tmc}$ would suggest that the subcortical and cortical factors were associated with different cognitive decline rates.

The results of the above statistical tests are illustrated in Figs. 5A2, 5B2, 7, S6A2, S6B2, S7A2, S7B2, S7C2, S8A2 and S8B2, where (except in Figs. 5A2 and 5B2) the blue dot corresponds to the estimated difference in cognitive decline rate between two "pure factors" after controlling for age, sex, education and total atrophy. For example, when comparing temporal and subcortical factors at the AD dementia stage, the estimated difference in cognitive decline rate is given by $\beta_{ts} + \beta_{tds}$. The red bar corresponds to the standard error of this estimation given by $SD(\beta_{ts} + \beta_{tds})$.

References

[1] Fischl B (2012) FreeSurfer. *NeuroImage* 62(2):774-781.

[2] Douaud G, et al. (2007) Anatomically related grey and white matter abnormalities in adolescent-onset schizophrenia. *Brain* 130(9):2375-2386.

[3] Gibbons LE, et al. (2012) A composite score for executive functioning, validated in Alzheimer's Disease Neuroimaging Initiative (ADNI) participants with baseline mild cognitive impairment. *Brain Imaging Behav* 6(4):517-527.

[4] Smith SM (2002) Fast robust automated brain extraction. *Hum Brain Map* 17(3):143-155.

[5] Koch KR (1999) *Parameter estimation and hypothesis testing in linear models*. Springer Sci & Business Media.

[6] Murray ME, et al. (2011) Neuropathologically defined subtypes of Alzheimer's disease with distinct clinical characteristics: a retrospective study. *Lancet Neurol* 10(9):785-796.

[7] Bernal-Rusiel JL, Greve DN, Reuter M, Fischl B, Sabuncu MR (2013) Statistical analysis of longitudinal neuroimage data with linear mixed effects models. *NeuroImage* 66:249-260.

[8] Crane PK, et al. (2012) Development and assessment of a composite score for memory in the Alzheimer's Disease Neuroimaging Initiative (ADNI). *Brain Imaging Behav* 6(4):502-516.

Supplemental Figures and Tables

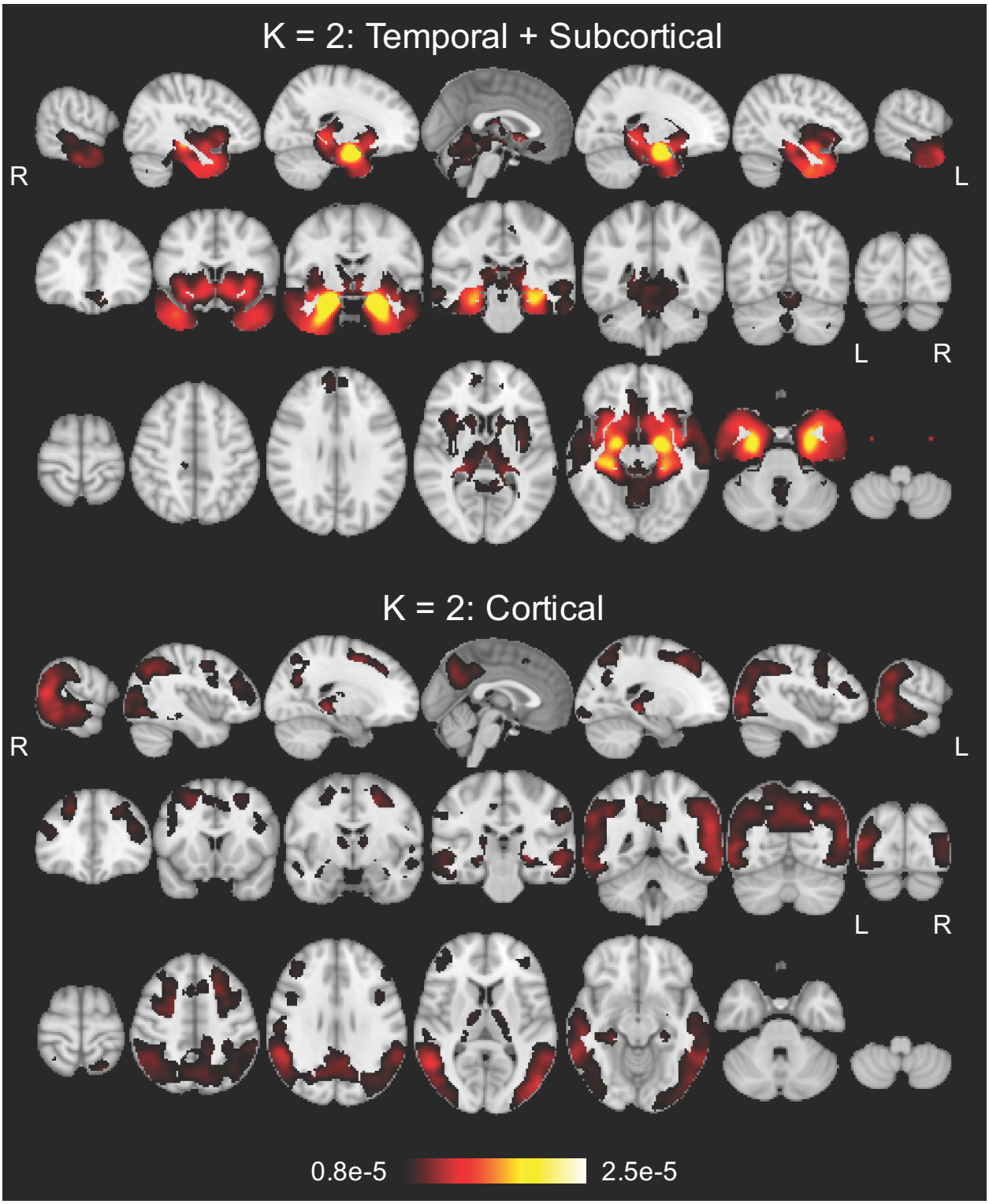

Fig. S1. Sagittal, coronal and axial slices of the probabilistic atrophy maps for K = 2, 3 and 4 atrophy factors. Bright color indicates high probability of atrophy at that spatial location for a particular atrophy factor, i.e., Pr(Voxel | Factor).

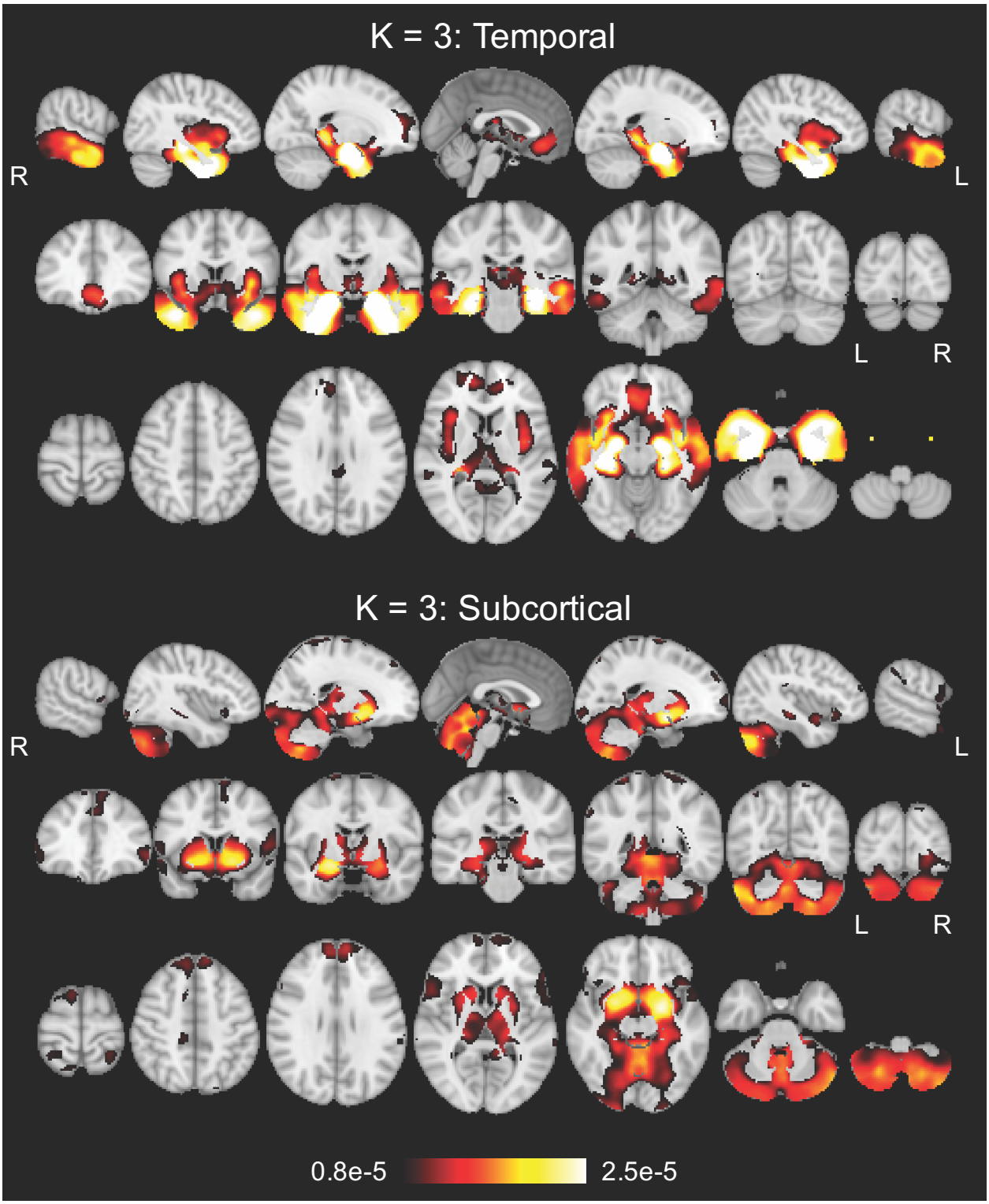

Fig. S1 (cont'd).

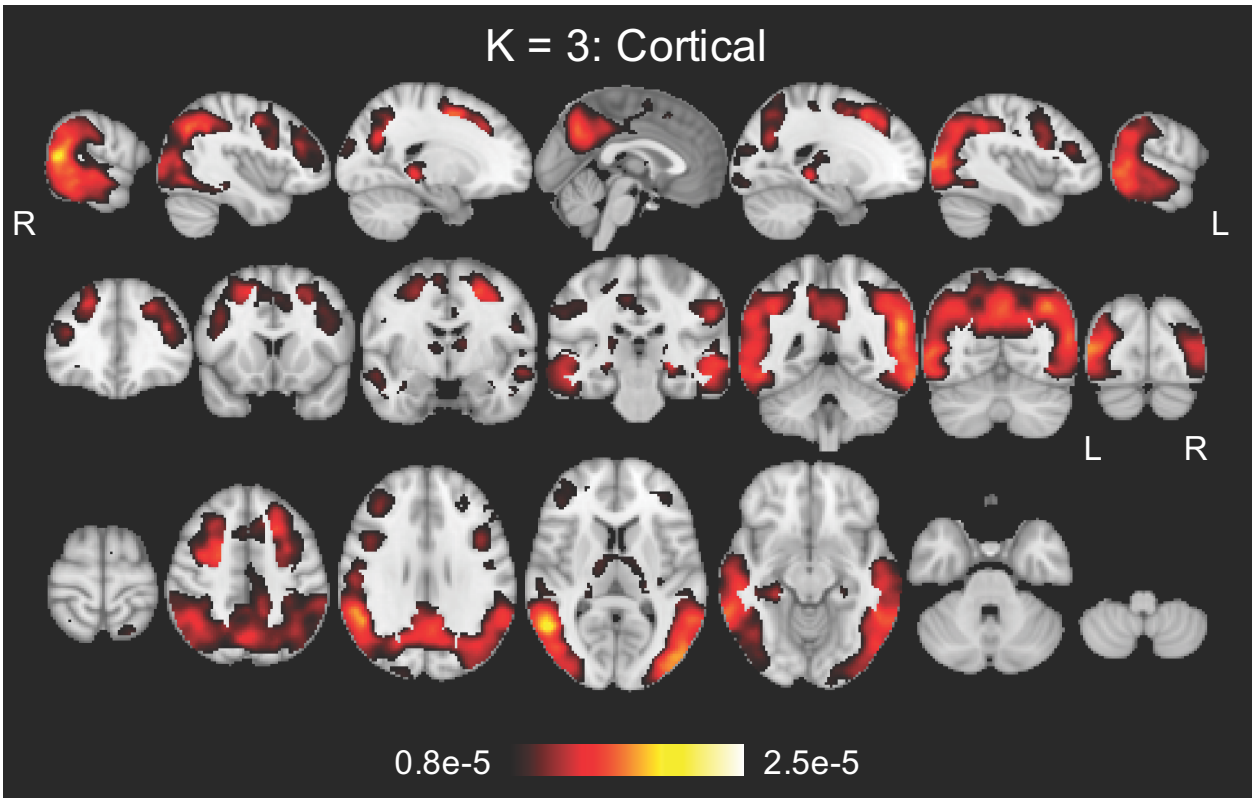

Fig. S1 (cont'd).

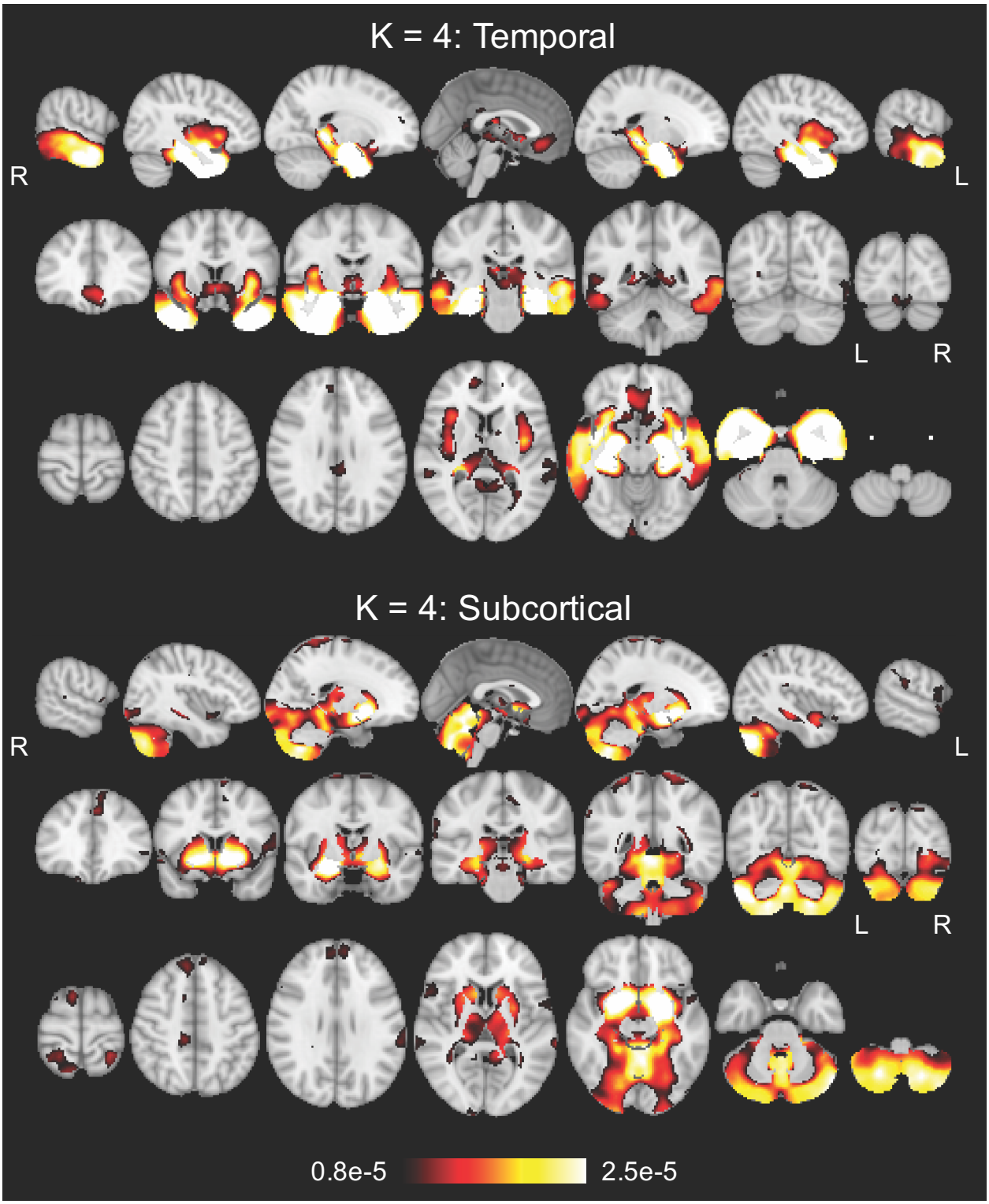

Fig. S1 (cont'd).

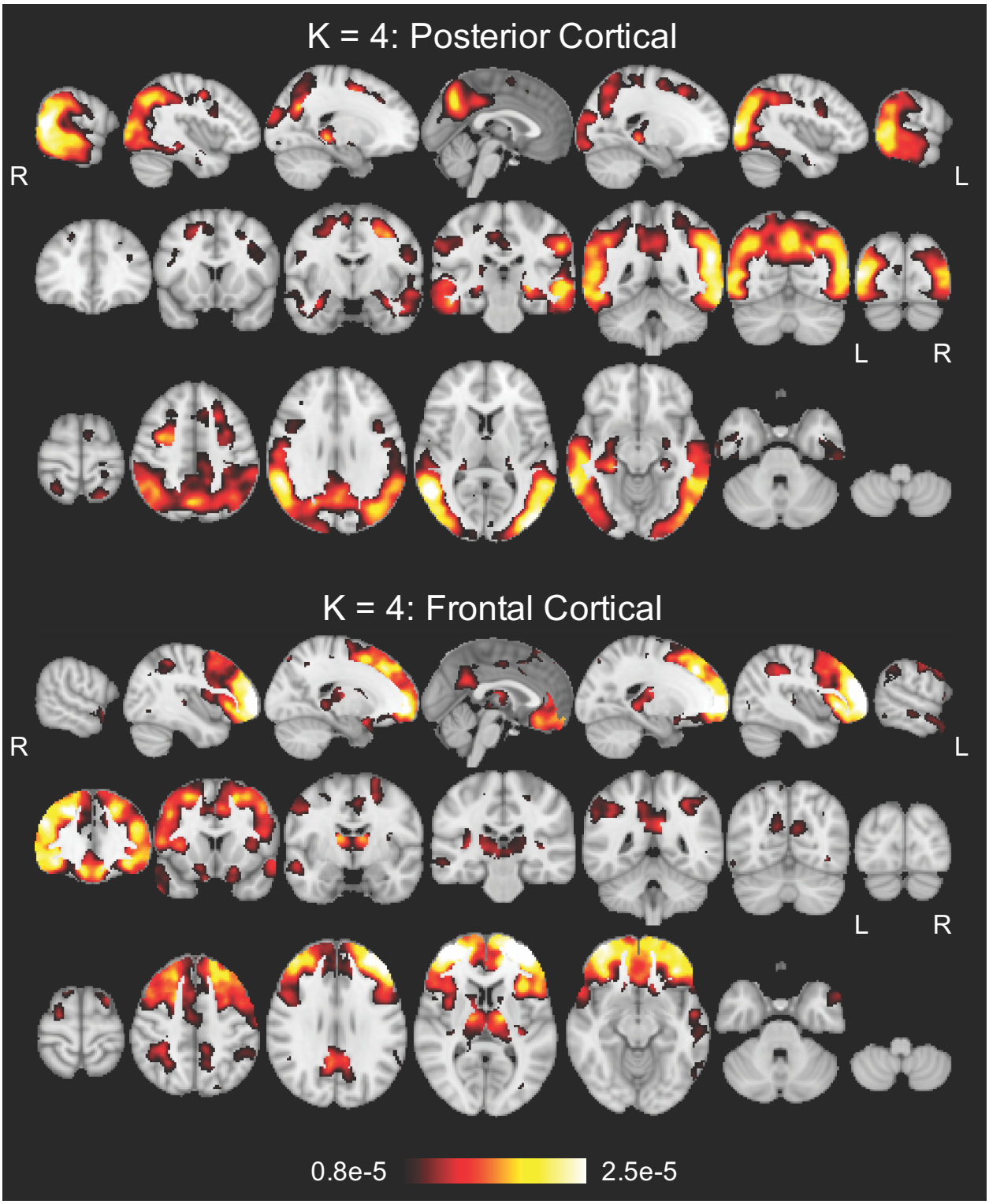
K = 4: Posterior Cortical
R
L
L
R
K = 4: Frontal Cortical
R
L
L
R
0.8e-5
2.5e-5

Fig. S1 (cont'd).

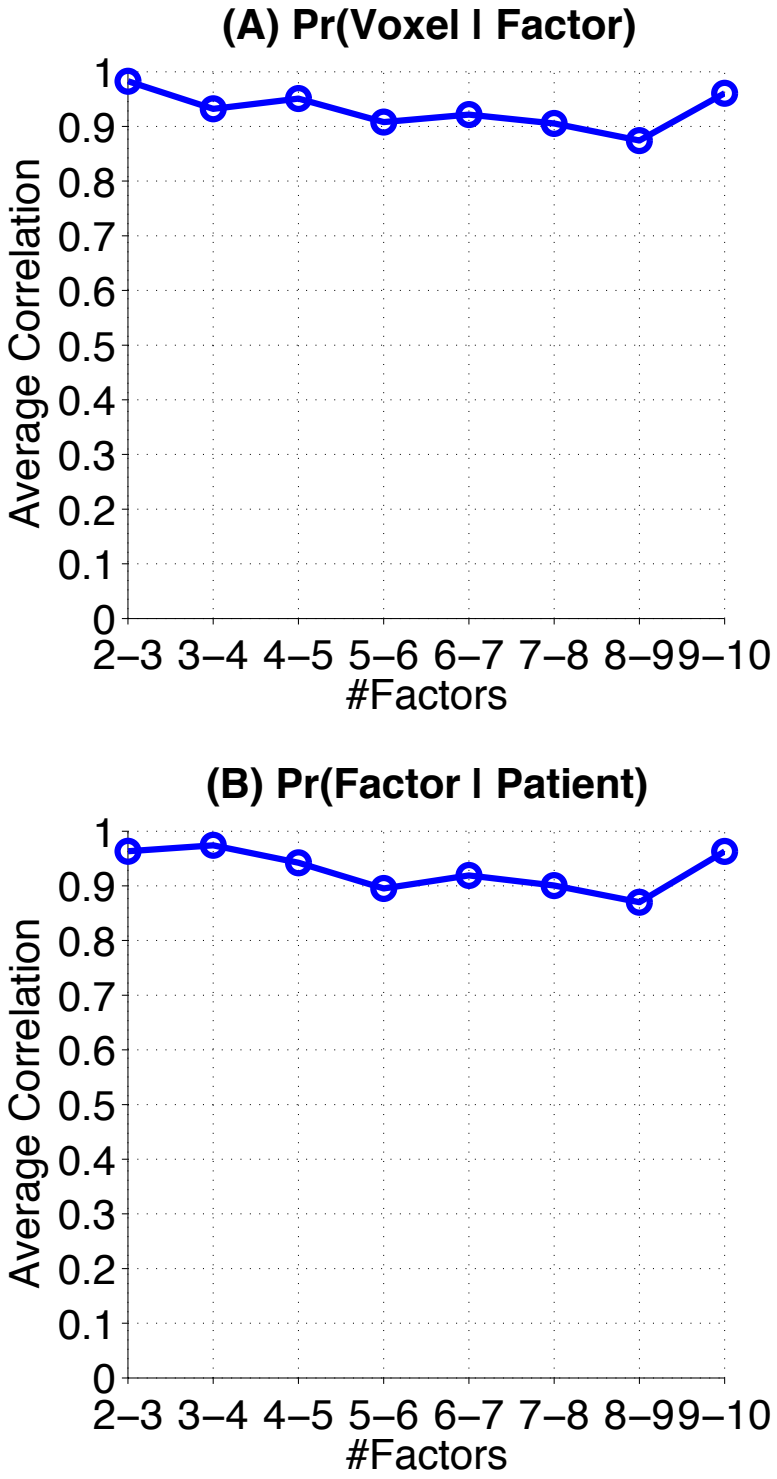

Fig. S2. Quantifying the nested hierarchy of latent atrophy factors in terms of (A) atrophy patterns and (B) individual factor compositions. A high correlation value at "K-(K+1)" on the x-axis indicates a high-quality split from the K-factor model to the (K+1)-factor model (see **Supplemental Methods** of **SI**). For example, the close-to-one values at "2-3" in both (A) and (B) suggest that the splits of both the atrophy patterns and individual factor compositions are high-quality from two to three atrophy factors. Overall, the high correlation values from 2 to 10 support a nested hierarchy of latent atrophy factors.

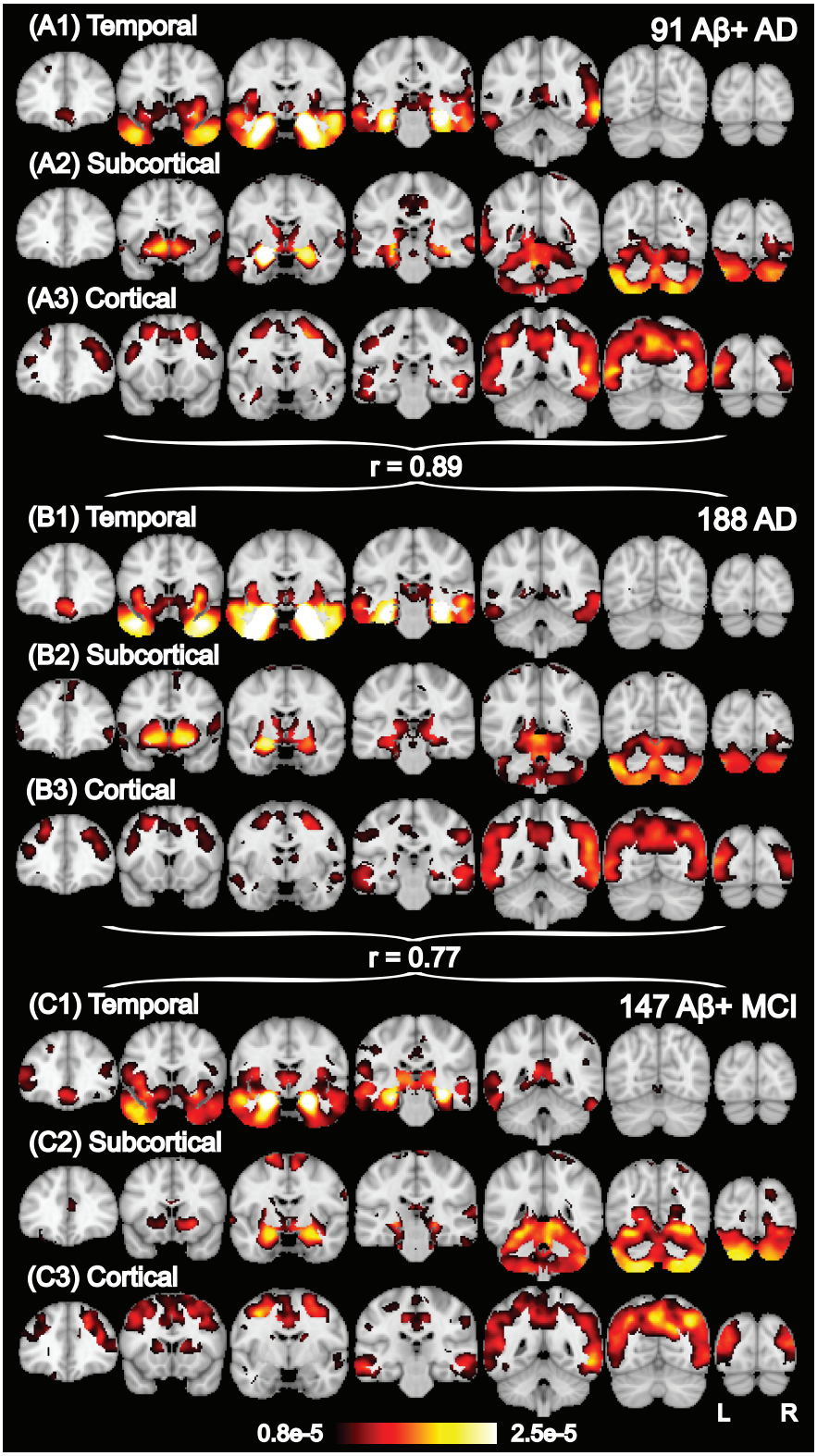

Fig. S3. Probabilistic atrophy maps for K = 3 factors estimated with (A) 91 Aβ+ AD dementia patients, (B) all 188 AD dementia patients, and (C) 147 Aβ+ MCI participants. The three different cohorts yielded highly similar atrophy patterns. Bright color indicates high probability of atrophy at that spatial location for a particular atrophy factor, i.e., Pr(Voxel | Factor).

FreeSurfer Structure Name	Average Probability
Right-Amygdala	3.81e-5
Left-Amygdala	3.59e-5
ctx-rh-entorhinal	3.03e-5
ctx-lh-entorhinal	2.87e-5
Right-Hippocampus	2.86e-5
Left-Hippocampus	2.51e-5
ctx-rh-parahippocampal	2.24e-5
ctx-lh-temporalpole	2.06e-5
ctx-rh-temporalpole	1.95e-5
ctx-lh-parahippocampal	1.78e-5
ctx-rh-inferiortemporal	1.52e-5
ctx-lh-middletemporal	1.50e-5
ctx-rh-middletemporal	1.47e-5
ctx-rh-fusiform	1.40e-5
ctx-lh-inferiortemporal	1.32e-5
ctx-lh-fusiform	1.26e-5
ctx-rh-insula	1.26e-5
ctx-lh-insula	1.20e-5
ctx-lh-superiortemporal	1.09e-5
ctx-lh-rostralanteriorcingulate	1.03e-5
ctx-rh-superiortemporal	9.82e-6
ctx-rh-medialorbitofrontal	8.39e-6
ctx-rh-rostralanteriorcingulate	7.77e-6
ctx-rh-lateralorbitofrontal	7.71e-6
ctx-lh-medialorbitofrontal	7.71e-6
ctx-rh-transversetemporal	7.13e-6
ctx-lh-lateralorbitofrontal	6.92e-6
Right-VentralDC	5.95e-6
ctx-lh-caudalanteriorcingulate	3.71e-6

Table S1A. Top anatomical structures associated with the temporal factor (see **Methods**). The temporal factor was associated with significantly greater atrophy in these structures than the subcortical factor ($p = 2e-15$) and cortical factor ($p = 4e-15$). There were no differences in atrophy of these structures between the subcortical and cortical factors ($p = 0.84$). See **Supplemental Methods** of **SI**.

FreeSurfer Structure Name	Average Probability
Right-Accumbens-area	1.85e-5
Left-Accumbens-area	1.75e-5
Right-Putamen	1.31e-5
Left-Cerebellum-Cortex	1.16e-5
Left-Putamen	1.13e-5
Right-Cerebellum-Cortex	1.10e-5
Left-Thalamus-Proper	8.82e-6
Right-Thalamus-Proper	7.99e-6
Right-Caudate	7.62e-6
ctx-lh-lingual	7.58e-6
Left-Caudate	7.50e-6
ctx-rh-lingual	7.16e-6
ctx-lh-parstriangularis	7.10e-6
ctx-rh-parstriangularis	6.52e-6
ctx-rh-parsopercularis	6.25e-6
ctx-rh-superiorfrontal	5.81e-6
ctx-rh-parsorbitalis	5.57e-6
Left-VentralDC	5.46e-6
ctx-lh-parsorbitalis	5.26e-6
ctx-lh-superiorfrontal	5.01e-6
ctx-lh-frontalpole	4.31e-6
ctx-rh-frontalpole	3.57e-6
Brain-Stem	3.36e-6
Right-Pallidum	2.55e-6
Left-Pallidum	2.22e-6

Table S1B. Top anatomical structures associated with the subcortical factor (see **Methods**). The subcortical factor was associated with significantly greater atrophy in these structures than the temporal factor ($p = 1e\text{-}5$) and cortical factor ($p = 2e\text{-}12$). The temporal factor had more atrophy in these structures than the cortical factor ($p = 0.01$). See **Supplemental Methods** of **SI**.

FreeSurfer Structure Name	Average Probability
ctx-lh-bankssts	1.15e-5
ctx-rh-inferiorparietal	1.10e-5
ctx-lh-precuneus	1.00e-5
ctx-rh-bankssts	9.92e-6
ctx-rh-precuneus	9.07e-6
ctx-lh-inferiorparietal	8.94e-6
ctx-lh-caudalmiddlefrontal	8.47e-6
ctx-rh-caudalmiddlefrontal	8.37e-6
ctx-rh-lateraloccipital	8.22e-6
ctx-lh-supramarginal	7.99e-6
ctx-lh-lateraloccipital	7.64e-6
ctx-rh-isthmuscingulate	7.32e-6
ctx-rh-cuneus	7.16e-6
ctx-lh-isthmuscingulate	7.11e-6
ctx-lh-superiorparietal	6.89e-6
ctx-rh-supramarginal	6.74e-6
ctx-lh-paracentral	6.53e-6
ctx-lh-cuneus	6.47e-6
ctx-lh-transversetemporal	6.29e-6
ctx-rh-posteriorcingulate	6.29e-6
ctx-lh-parsopercularis	6.05e-6
ctx-lh-posteriorcingulate	5.87e-6
ctx-lh-rostralmiddlefrontal	5.69e-6
ctx-rh-precentral	5.69e-6
ctx-rh-superiorparietal	5.57e-6
ctx-rh-rostralmiddlefrontal	5.41e-6
ctx-lh-precentral	5.33e-6
ctx-lh-pericalcarine	5.29e-6
ctx-lh-postcentral	5.27e-6
ctx-rh-pericalcarine	4.94e-6
ctx-rh-postcentral	4.73e-6
ctx-rh-paracentral	4.68e-6
ctx-rh-caudalanteriorcingulate	3.83e-6

Table S1C. Top anatomical structures associated with the cortical factor (see **Methods**). The cortical factor was associated with significantly greater atrophy in these structures than the temporal factor ($p = 7e-6$) and subcortical factor ($p = 4e-7$). There were no differences in atrophy of these structures between the temporal and subcortical factors ($p = 0.62$). See **Supplemental Methods** of **SI**.

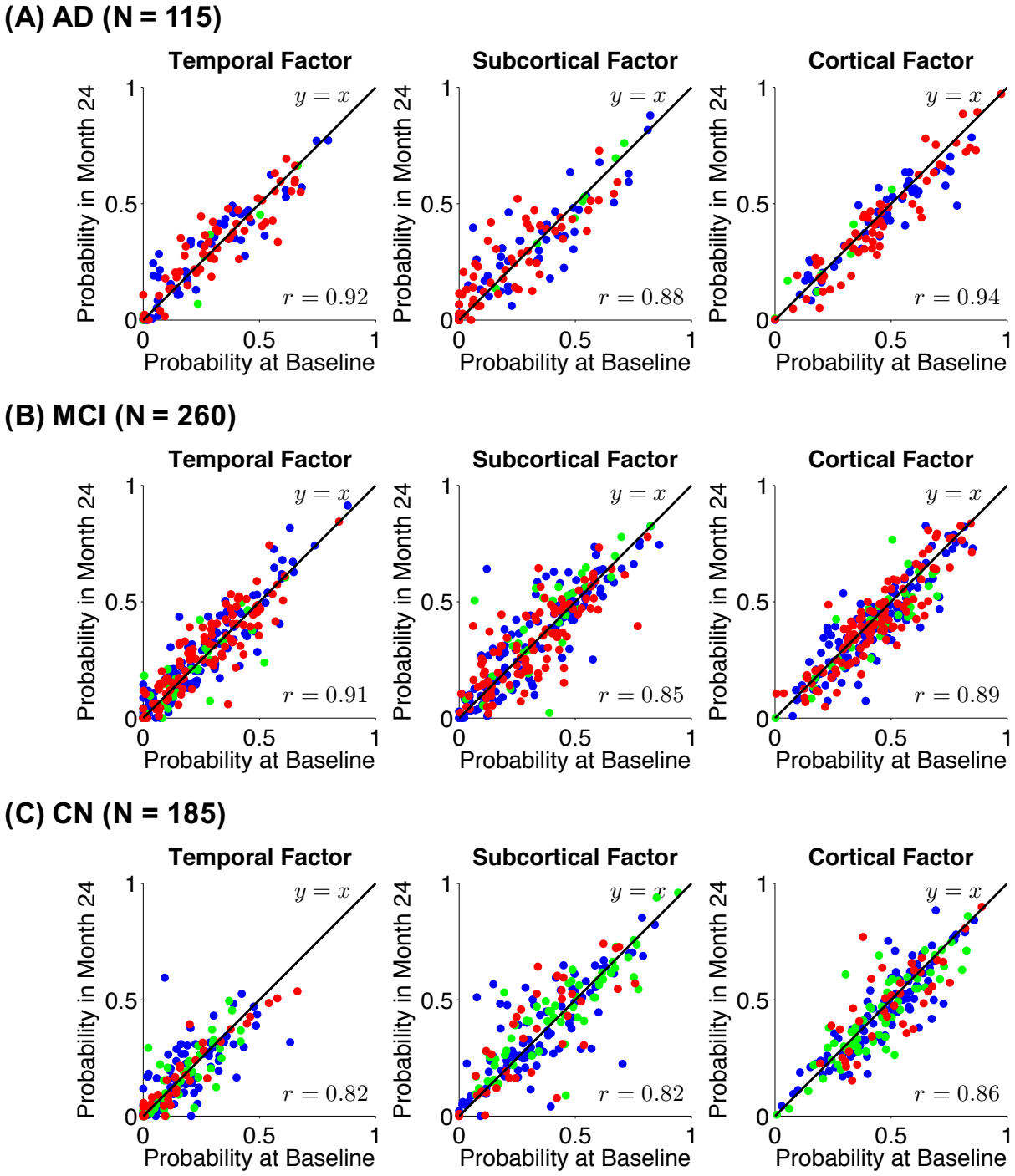

Fig. S4. Stability of factor compositions over two years for (A) 115 AD dementia patients, (B) 260 MCI participants, and (C) 185 CN participants. Each participant corresponds to a dot, whose color indicates amyloid status: red for Aβ+, green for Aβ-, and blue for unknown. For each atrophy factor (plot), x-axis and y-axis represent, respectively, the probabilities of factor at baseline and two years after baseline. In the ideal case where factor probability estimations remain exactly the same after two years, one would expect a y = x linear fit as well as a r = 1 correlation. In our case, the linear fits were close to y = x with r > 0.82 for all three atrophy factors for all clinical groups, suggesting that the factor compositions were stable despite disease progression.

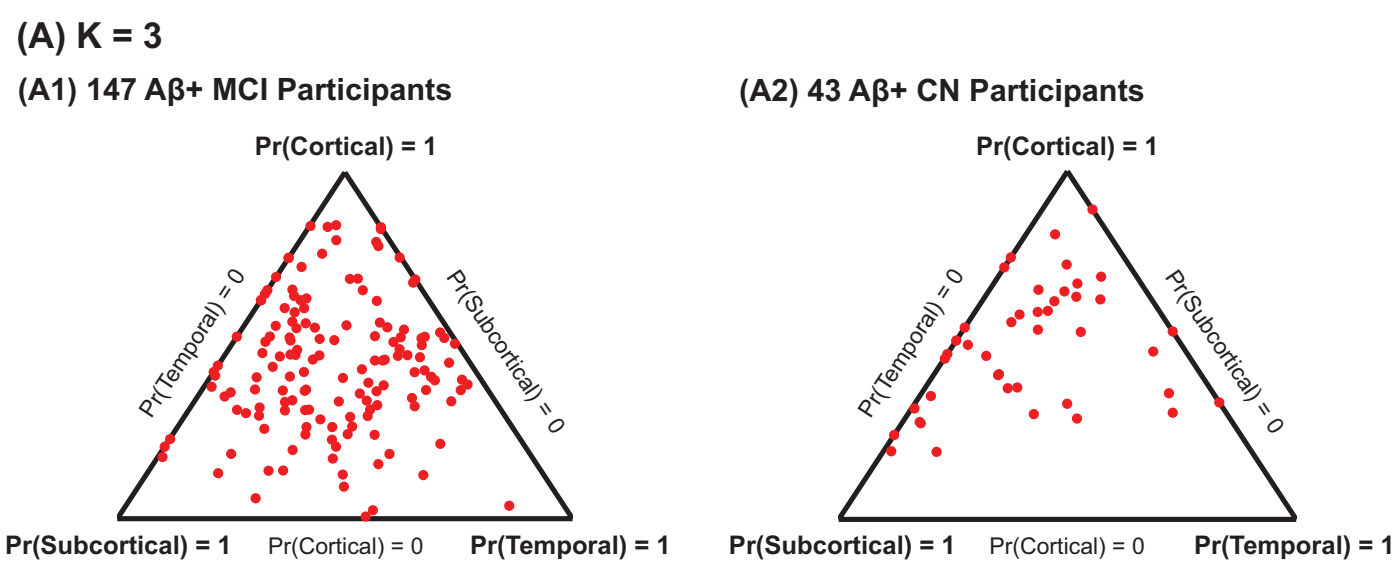

Fig. S5A. Factor compositions of (1) 147 Aβ+ MCI participants and (2) 43 Aβ+ CN participants for K = 3 factors. Each participant corresponds to a dot, whose location (in barycentric coordinates) represents the factor composition. Corners of the triangle represent "pure factors"; closer distance to the respective corners indicates higher probabilities for the respective factors. Most dots are far from the corners, suggesting that most participants expressed multiple factors.

(B) K = 2

(B1) 188 AD Dementia Patients

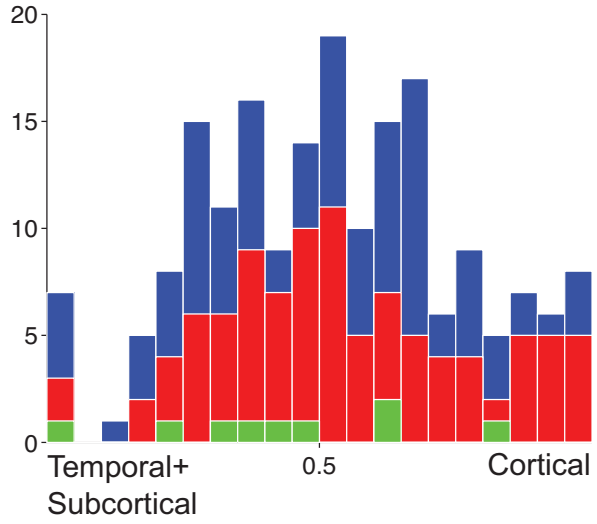

(B2) 147 Aβ+ MCI Participants

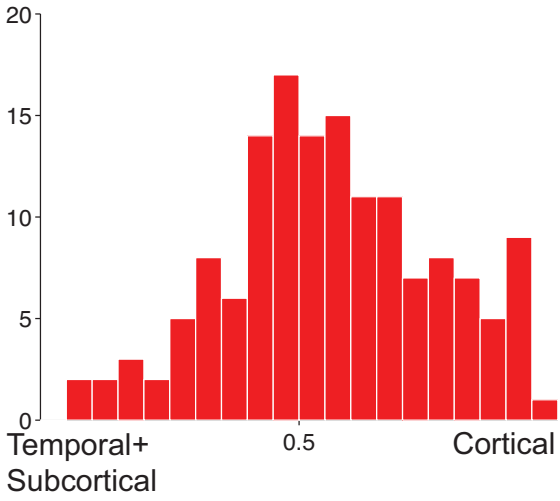

(B3) 43 Aβ+ CN Participants

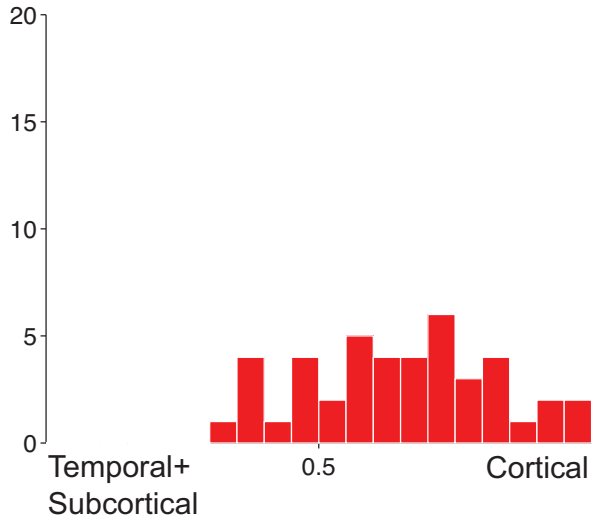

Fig. S5B. Factor compositions of (1) 188 AD dementia patients, (2) 147 Aβ+ MCI participants, and (3) 43 Aβ+ CN participants for K = 2 factors. Histograms were created with participants' cortical factor probability (x-axis). Therefore the left (or right) extreme corresponds to the pure temporal+subcortical (or cortical) factor. In addition, colors in (1) indicate amyloid status: red for Aβ+, green for Aβ-, and blue for unknown. The majority of the population lies around the center, suggesting that most participants expressed both atrophy factors.

(C) K = 4

(C1) 188 AD Dementia Patients

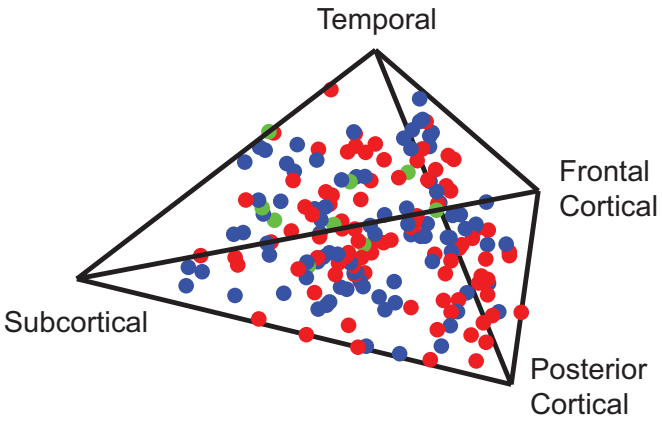

(C2) 147 Aβ+ MCI Participants

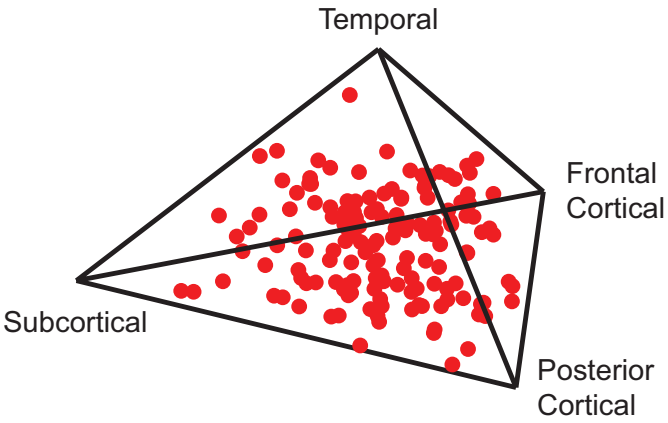

(C3) 43 Aβ+ CN Participants

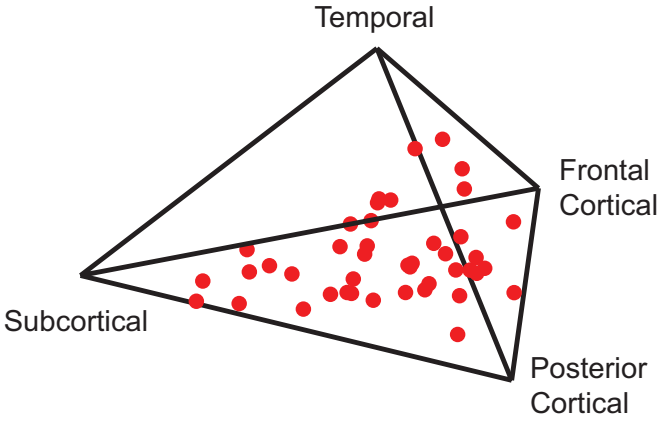

Fig. S5C. Factor compositions of (1) 188 AD dementia patients, (2) 147 Aβ+ MCI participants, and (3) 43 Aβ+ CN participants for K = 4 factors. Each participant corresponds to a dot, whose location represents the factor composition. Tetrahedron corners represent "pure factors"; closer distance to a corner corresponds to higher probability for the corresponding factor. Color in (1) indicates amyloid status: red for Aβ+, green for Aβ-, and blue for unknown. Most dots are far from the corners, suggesting that most participants expressed multiple factors.

	Temporal	Subcortical	Cortical	Overall p*
Baseline age (years)	76 (6.9)	76 (7.1)	74 (7.8)	**8e-7**
Age at AD onset (years)†	72 (7.5)	73 (7.7)	70 (8.5)	**1e-5**
Years from onset to baseline†	3.8 (2.6)	3.5 (2.4)	3.5 (2.4)	0.29
Education (years)	15 (3.1)	14 (3.1)	15 (3.2)	0.15
Sex (0 for male)	0.4 (0.5)	0.5 (0.5)	0.5 (0.5)	0.27
Amyloid (pg/mL)‡	141 (39)	149 (51)	140 (36)	0.09
APOE ε2§	0.03 (0.2)	0.08 (0.3)	0.04 (0.2)	0.03
APOE ε4§	0.86 (0.7)	0.81 (0.7)	0.87 (0.7)	0.61

Table S2. Characteristics of 188 AD dementia patients by factor. Data are weighted averages (weighted standard deviation) with weights corresponding to factor probabilities. Highlighted p values (blue) are characteristics significantly different across factors. *Computed by linear hypothesis test on GLM or likelihood ratio test on logistic regression for sex (see **Methods**). †Only available for 182 patients. ‡Only available for 100 patients. §The original counts were 0, 1 or 2.

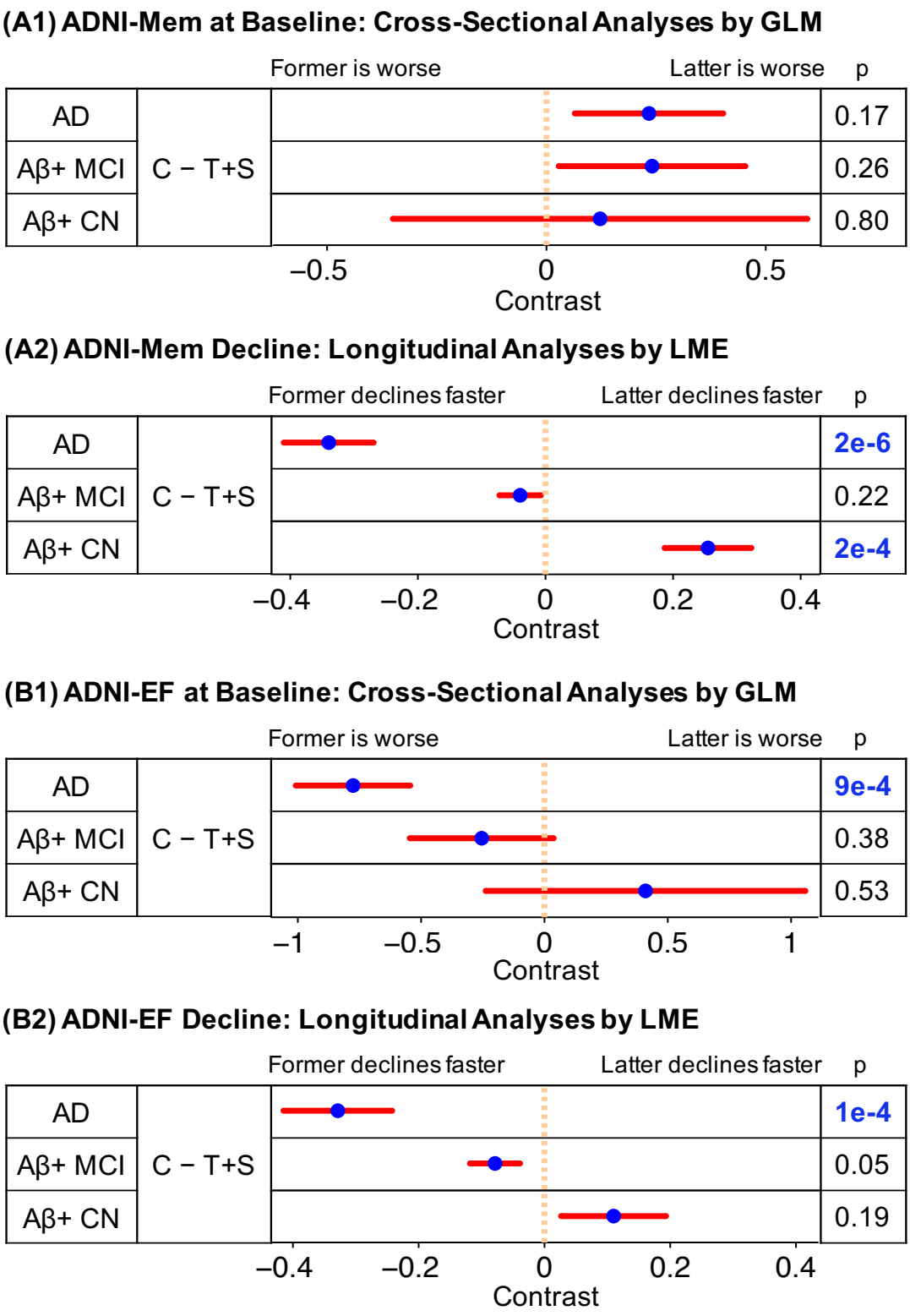

Fig. S6. Comparisons of (1) cross-sectional baseline and (2) longitudinal decline rates of (A) memory and (B) executive function between K = 2 factors. Comparisons remaining significant after FDR control (q = 0.05) are highlighted in blue. Blue dots are estimated differences between "pure atrophy factors", and red bars show the standard errors (see **Methods** and **Supplemental Methods** of **SI**).

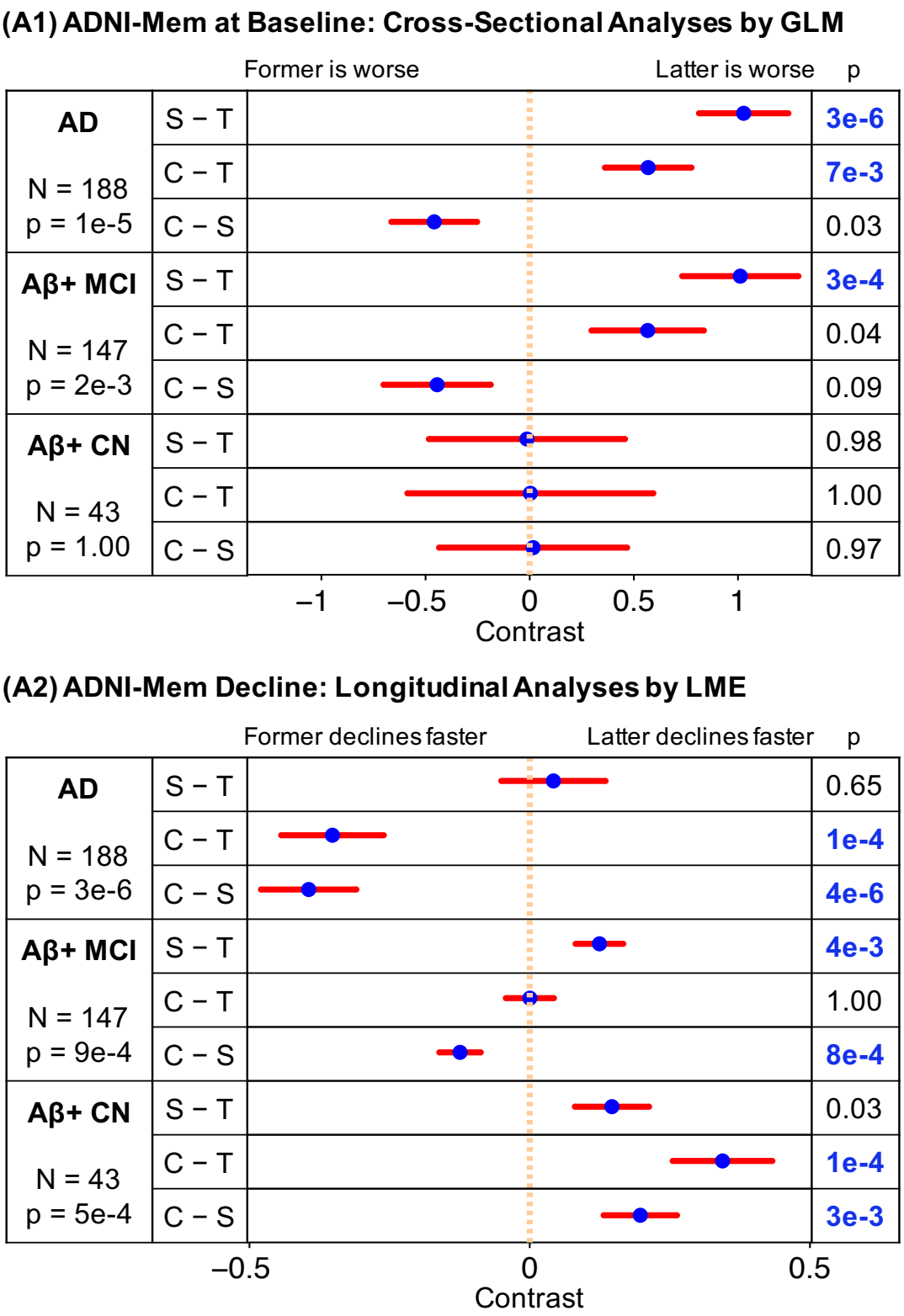

Fig. S7A. Comparisons of (1) cross-sectional baseline and (2) longitudinal decline rates of memory among K = 3 factors. Comparisons remaining significant after FDR control (q = 0.05) are highlighted in blue. Blue dots are estimated differences between "pure atrophy factors", and red bars show the standard errors (see **Methods** and **Supplemental Methods** of **SI**).

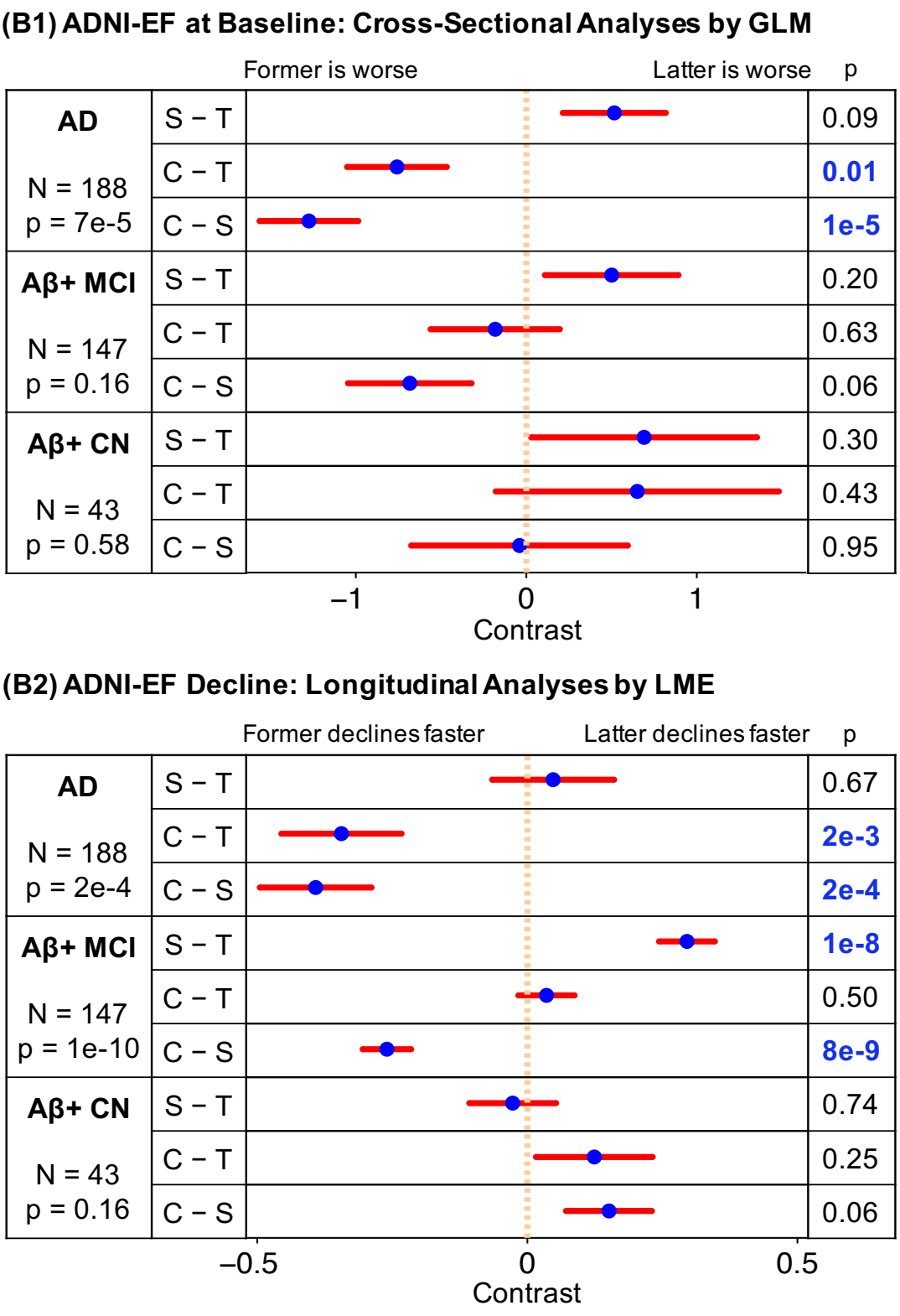

Fig. S7B. Comparisons of (1) cross-sectional baseline and (2) longitudinal decline rates of executive function among K = 3 factors. Comparisons remaining significant after FDR control (q = 0.05) are highlighted in blue. Blue dots are estimated differences between "pure atrophy factors", and red bars show the standard errors (see **Methods** and **Supplemental Methods** of **SI**).

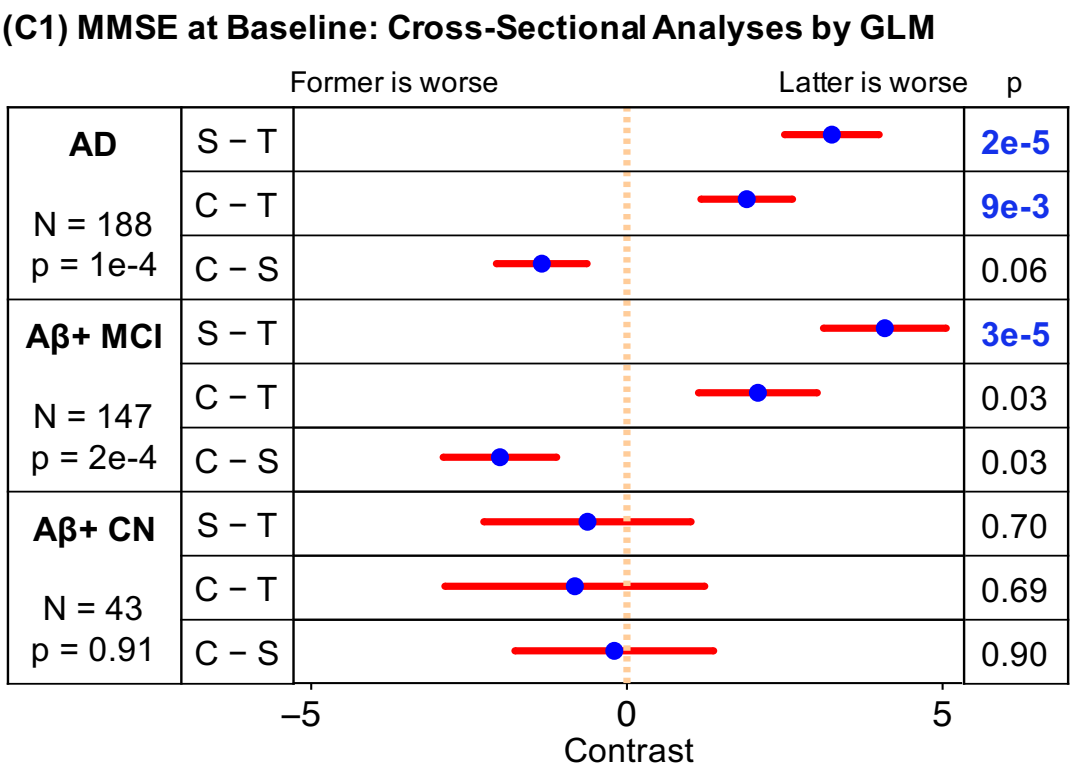

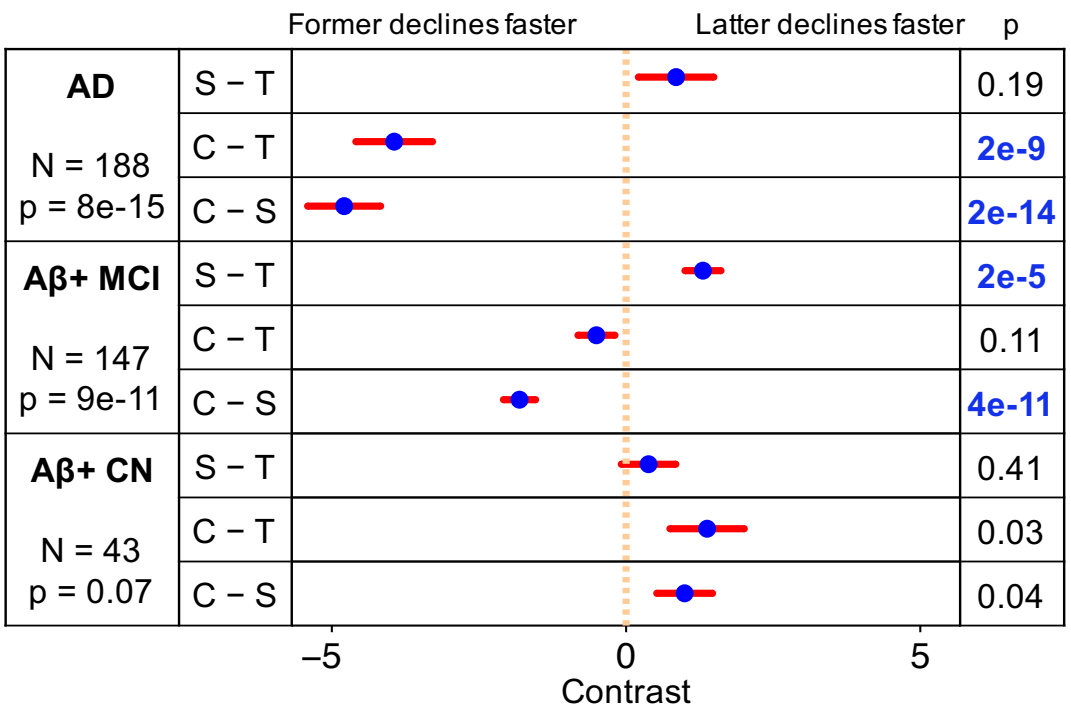

Fig. S7C. Comparisons of (1) cross-sectional baseline and (2) longitudinal decline rates of MMSE among K = 3 factors. Comparisons remaining significant after FDR control (q = 0.05) are highlighted in blue. Blue dots are estimated differences between "pure atrophy factors", and red bars show the standard errors (see **Methods** and **Supplemental Methods** of **SI**).

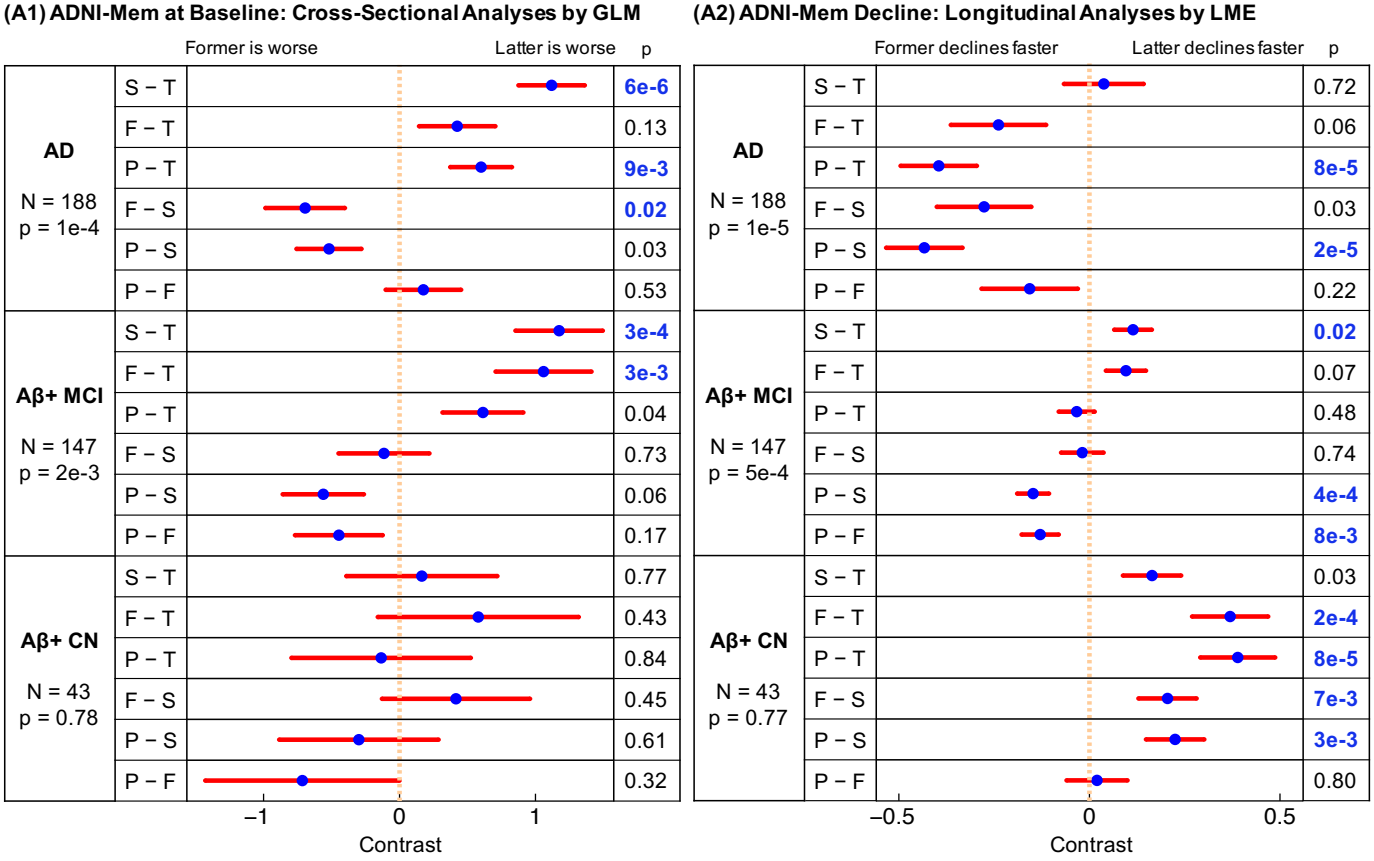

Fig. S8A. Comparisons of (1) cross-sectional baseline and (2) longitudinal decline rates of memory among K = 4 factors. Comparisons remaining significant after FDR control (q = 0.05) are highlighted in blue. Blue dots are estimated differences between "pure atrophy factors", and red bars show the standard errors (see **Methods** and **Supplemental Methods** of **SI**).

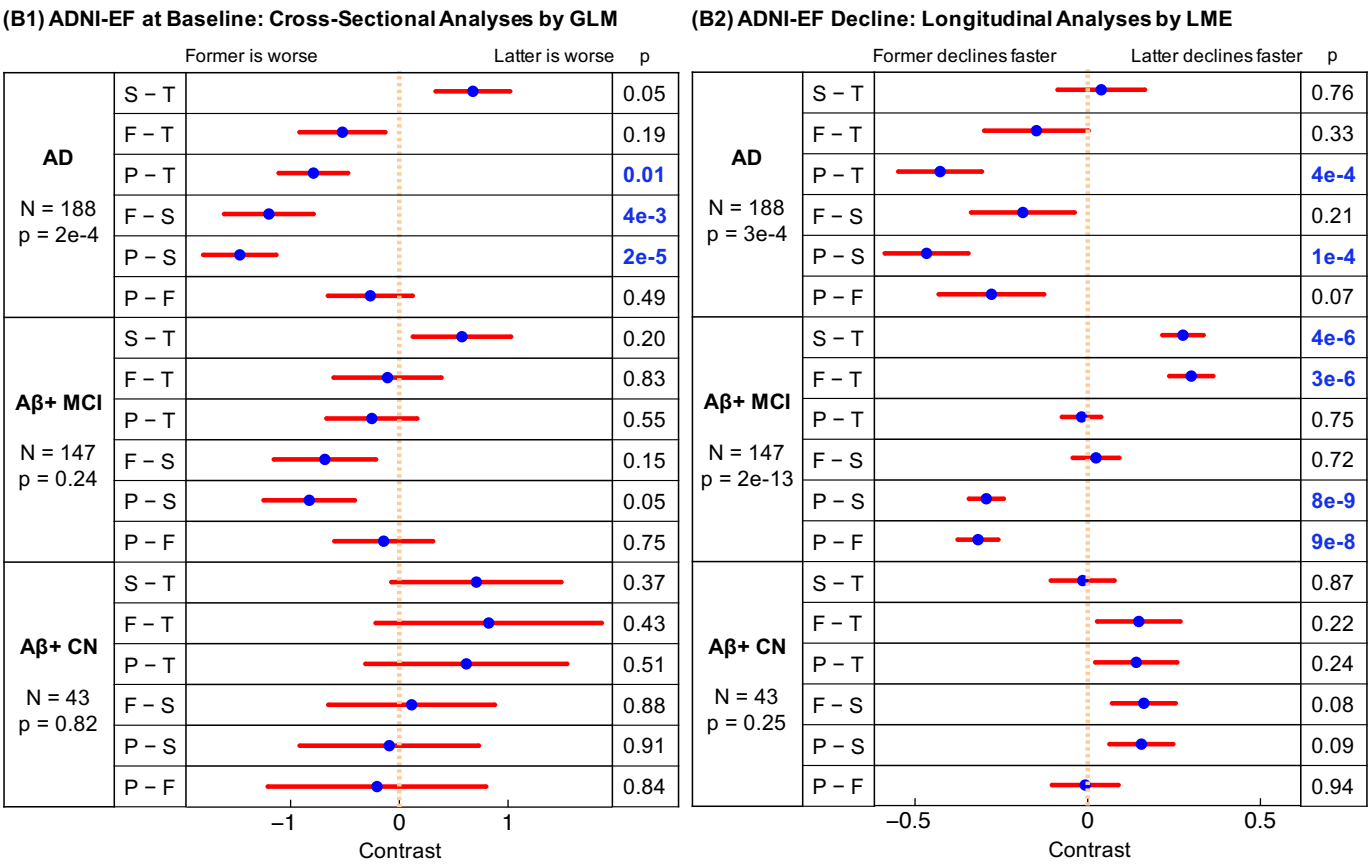

Fig. S8B. Comparisons of (1) cross-sectional baseline and (2) longitudinal decline rates of executive function among K = 4 factors. Comparisons remaining significant after FDR control (q = 0.05) are highlighted in blue. Blue dots are estimated differences between "pure atrophy factors", and red bars show the standard errors (see **Methods** and **Supplemental Methods** of **SI**).

Complete List of ADNI Investigators and Participating Institutions

ADNI Investigators

The following list is also available online at http://adni.loni.usc.edu/wp-content/uploads/how_to_apply/ADNI_Acknowledgement_List.pdf.

Part A: Leadership and Infrastructure

Principal Investigator

Michael W. Weiner, MD	UC San Francisco

ADCS PI and Director of Coordinating Center Clinical Core

Paul Aisen, MD	University of Southern California

Executive Committee

Michael Weiner, MD	UC San Francisco
Paul Aisen, MD	University of Southern California
Ronald Petersen, MD, PhD	Mayo Clinic, Rochester
Clifford R. Jack, Jr., MD	Mayo Clinic, Rochester
William Jagust, MD	UC Berkeley
John Q. Trojanowki, MD, PhD	U Pennsylvania
Arthur W. Toga, PhD	USC
Laurel Beckett, PhD	UC Davis
Robert C. Green, MD, MPH	Brigham and Women's Hospital/Harvard Medical School
Andrew J. Saykin, PsyD	Indiana University
John Morris, MD	Washington University St. Louis
Leslie M. Shaw	University of Pennsylvania

ADNI External Advisory Board (ESAB)

Zaven Khachaturian, PhD	Prevent Alzheimer's Disease 2020 (Chair)
Greg Sorensen, MD	Siemens
Maria Carrillo, PhD	Alzheimer's Association
Lew Kuller, MD	University of Pittsburgh
Marc Raichle, MD	Washington University St. Louis
Steven Paul, MD	Cornell University
Peter Davies, MD	Albert Einstein College of Medicine of Yeshiva University
Howard Fillit, MD	AD Drug Discovery Foundation
Franz Hefti, PhD	Acumen Pharmaceuticals
David Holtzman, MD	Washington University St. Louis
M. Marcel Mesulam, MD	Northwestern University
William Potter, MD	National Institute of Mental Health
Peter Snyder, PhD	Brown University

ADNI 2 Private Partner Scientific Board (PPSB)

Adam Schwartz, MD	Eli Lilly (Chair)

Data and Publications Committee

Robert C. Green, MD, MPH	BWH/HMS (Chair)

Resource Allocation Review Committee

Tom Montine, MD, PhD	University of Washington (Chair)

Clinical Core Leaders

Ronald Petersen, MD, PhD	Mayo Clinic, Rochester (Core PI)
Paul Aisen, MD	University of Southern California

Clinical Informatics and Operations

Ronald G. Thomas, PhD	UC San Diego
Michael Donohue, PhD	UC San Diego
Sarah Walter, MSc	UC San Diego
Devon Gessert	UC San Diego
Tamie Sather, MA	UC San Diego
Gus Jiminez, MBS	UC San Diego
Archana B. Balasubramanian, PhD	UC San Diego
Jennifer Mason, MPH	UC San Diego
Iris Sim	UC San Diego

Biostatistics Core Leaders and Key Personnel

Laurel Beckett, PhD	UC Davis (Core PI)
Danielle Harvey, PhD	UC Davis
Michael Donohue, PhD	UC San Diego

MRI Core Leaders and Key Personnel

Clifford R. Jack, Jr., MD	Mayo Clinic, Rochester (Core PI)
Matthew Bernstein, PhD	Mayo Clinic, Rochester
Nick Fox, MD	University of London
Paul Thompson, PhD	UCLA School of Medicine
Norbert Schuff, PhD	UCSF MRI
Charles DeCArli, MD	UC Davis
Bret Borowski, RT	Mayo Clinic
Jeff Gunter, PhD	Mayo Clinic
Matt Senjem, MS	Mayo Clinic
Prashanthi Vemuri, PhD	Mayo Clinic
David Jones, MD	Mayo Clinic
Kejal Kantarci	Mayo Clinic
Chad Ward	Mayo Clinic

PET Core Leaders and Key Personnel

William Jagust, MD	UC Berkeley (Core PI)
Robert A. Koeppe, PhD	University of Michigan
Norm Foster, MD	University of Utah
Eric M. Reiman, MD	Banner Alzheimer's Institute
Kewei Chen, PhD	Banner Alzheimer's Institute
Chet Mathis, MD	University of Pittsburgh
Susan Landau, PhD	UC Berkeley

Neuropathology Core Leaders

John C. Morris, MD	Washington University St. Louis
Nigel J. Cairns, PhD, FRCPath	Washington University St. Louis
Erin Franklin, MS, CCRP	Washington University St. Louis
Lisa Taylor-Reinwald, BA, HTL (ASCP) – Past Investigator	Washington University St. Louis

Biomarkers Core Leaders and Key Personnel

Leslie M. Shaw, PhD	UPenn School of Medicine
John Q. Trojanowki, MD, PhD	UPenn School of Medicine
Virginia Lee, PhD, MBA	UPenn School of Medicine
Magdalena Korecka, PhD	UPenn School of Medicine
Michal Figurski, PhD	UPenn School of Medicine

Informatics Core Leaders and Key Personnel

Arthur W. Toga, PhD	USC (Core PI)
Karen Crawford	USC
Scott Neu, PhD	USC

Genetics Core Leaders and Key Personnel

Andrew J. Saykin, PsyD	Indiana University
Tatiana M. Foroud, PhD	Indiana University
Steven Potkin, MD UC	UC Irvine
Li Shen, PhD	Indiana University
Kelley Faber, MS, CCRC	Indiana University
Sungeun Kim, PhD	Indiana University
Kwangsik Nho, PhD	Indiana University

Initial Concept Planning & Development

Michael W. Weiner, MD	UC San Francisco
Lean Thal, MD	UC San Diego
Zaven Khachaturian, PhD	Prevent Alzheimer's Disease 2020

Early Project Proposal Development

Leon Thal, MD	UC San Diego
Neil Buckholtz	National Institute on Aging
Michael W. Weiner, MD	UC San Francisco
Peter J. Snyder, PhD	Brown University
William Potter, MD	National Institute of Mental Health
Steven Paul, MD	Cornell University
Marilyn Albert, PhD	Johns Hopkins University
Richard Frank, MD, PhD	Richard Frank Consulting
Zaven Khachaturian, PhD	Prevent Alzheimer's Disease 2020

NIA

John Hsiao, MD	National Institute on Aging

Part B: Investigators By Site

Oregon Health & Science University:
Jeffrey Kaye, MD
Joseph Quinn, MD
Lisa Silbert, MD
Betty Lind, BS
Raina Carter, BA – Past Investigator
Sara Dolen, BS – Past Investigator

University of Southern California:
Lon S. Schneider, MD
Sonia Pawluczyk, MD
Mauricio Becerra, BS
Liberty Teodoro, RN
Bryan M. Spann, DO, PhD – Past Investigator

University of California – San Diego:
James Brewer, MD, PhD
Helen Vanderswag, RN
Adam Fleisher, MD – Past Investigator

University of Michigan:
Judith L. Heidebrink, MD, MS
Joanne L. Lord, LPN, BA, CCRC – Past Investigator

Mayo Clinic, Rochester:
Ronald Petersen, MD, PhD
Sara S. Mason, RN
Colleen S. Albers, RN
David Knopman, MD
Kris Johnson, RN – Past Investigator

Baylor College of Medicine:
Rachelle S. Doody, MD, PhD
Javier Villanueva-Meyer, MD
Valory Pavlik, PhD
Victoria Shibley, MS
Munir Chowdhury, MBBS, MS – Past Investigator
Susan Rountree, MD – Past Investigator
Mimi Dang, MD – Past Investigator

Columbia University Medical Center:
Yaakov Stern, PhD
Lawrence S. Honig, MD, PhD
Karen L. Bell, MD

Washington University, St. Louis:
Beau Ances, MD
John C. Morris, MD
Maria Carroll, RN, MSN
Mary L. Creech, RN, MSW
Erin Franklin, MS, CCRP
Mark A. Mintun, MD – Past Investigator
Stacy Schneider, APRN, BC, GNP – Past Investigator
Angela Oliver, RN, BSN, MSG – Past Investigator

University of Alabama - Birmingham:
Daniel Marson, JD, PhD
David Geldmacher, MD
Marissa Natelson Love, MD
Randall Griffith, PhD, ABPP – Past Investigator
David Clark, MD – Past Investigator
John Brockington, MD – Past Investigator
Erik Roberson, MD – Past Investigator

Mount Sinai School of Medicine:
Hillel Grossman, MD
Effie Mitsis, PhD

Rush University Medical Center:
Raj C. Shah, MD
Leyla deToledo-Morrell, PhD – Past Investigator

Wien Center:
Ranjan Duara, MD
Maria T. Greig-Custo, MD
Warren Barker, MA, MS

Johns Hopkins University:
Marilyn Albert, PhD
Chiadi Onyike, MD
Daniel D'Agostino II, BS
Stephanie Kielb, BS – Past Investigator

New York University:
Martin Sadowski, MD, PhD
Mohammed O. Sheikh, MD
Anaztasia Ulysse
Mrunalini Gaikwad

Duke University Medical Center:
P. Murali Doraiswamy, MBBS, FRCP
Jeffrey R. Petrella, MD

Salvador Borges-Neto, MD
Terence Z. Wong, MD – Past Investigator
Edward Coleman – Past Investigator

University of Pennsylvania:
Steven E. Arnold, MD
Jason H. Karlawish, MD
David A. Wolk, MD
Christopher M. Clark, MD

University of Kentucky:
Charles D. Smith, MD
Greg Jicha, MD
Peter Hardy, PhD
Partha Sinha, PhD
Elizabeth Oates, MD
Gary Conrad, MD

University of Pittsburgh:
Oscar L. Lopez, MD
MaryAnn Oakley, MA
Donna M. Simpson, CRNP, MPH

University of Rochester Medical Center:
Anton P. Porsteinsson, MD
Bonnie S. Goldstein, MS, NP
Kim Martin, RN
Kelly M. Makino, BS – Past Investigator
M. Saleem Ismail, MD – Past Investigator
Connie Brand, RN – Past Investigator

University of California, Irvine:
Steven G. Potkin, MD
Adrian Preda, MD
Dana Nguyen, PhD

University of Texas Southwestern Medical School:
Kyle Womack, MD
Dana Mathews, MD, PhD
Mary Quiceno, MD

Emory University:
Allan I. Levey, MD, PhD
James J. Lah, MD, PhD
Janet S. Cellar, DNP, PMHCNS-BC

University of Kansas, Medical Center:
Jeffrey M. Burns, MD
Russell H. Swerdlow, MD
William M. Brooks, PhD

University of California, Los Angeles:
Liana Apostolova, MD
Kathleen Tingus, PhD
Ellen Woo, PhD
Daniel H.S. Silverman, MD, PhD
Po H. Lu, PsyD – Past Investigator
George Bartzokis, MD – Past Investigator

Mayo Clinic, Jacksonville:
Neill R Graff-Radford, MBBCH, FRCP (London)
Francine Parfitt, MSH, CCRC
Kim Poki-Walker, BA

Indiana University:
Martin R. Farlow, MD
Ann Marie Hake, MD
Brandy R. Matthews, MD – Past Investigator
Jared R. Brosch, MD
Scott Herring, RN, CCRC

Yale University School of Medicine:
Christopher H. van Dyck, MD
Richard E. Carson, PhD
Martha G. MacAvoy, PhD
Pradeep Varma, MD

McGill Univ., Montreal-Jewish General Hospital:
Howard Chertkow, MD
Howard Bergman, MD
Chris Hosein, MEd

Sunnybrook Health Sciences, Ontario:
Sandra Black, MD, FRCPC
Bojana Stefanovic, PhD
Curtis Caldwell, PhD

U.B.C. Clinic for AD & Related Disorders:
Ging-Yuek Robin Hsiung, MD, MHSc, FRCPC
Benita Mudge, BS
Vesna Sossi, PhD
Howard Feldman, MD, FRCPC – Past Investigator
Michele Assaly, MA – Past Investigator

Cognitive Neurology - St. Joseph's, Ontario:
Elizabeth Finger, MD
Stephen Pasternack, MD, PhD
Irina Rachisky, MD
Dick Trost, PhD – Past Investigator

Andrew Kertesz, MD – Past Investigator

Cleveland Clinic Lou Ruvo Center for Brain Health:
Charles Bernick, MD, MPH
Donna Munic, PhD

Northwestern University:
Marek-Marsel Mesulam, MD
Emily Rogalski, PhD
Kristine Lipowski, MA
Sandra Weintraub, PhD
Borna Bonakdarpour, MD
Diana Kerwin, MD – Past Investigator
Chuang-Kuo Wu, MD, PhD – Past Investigator
Nancy Johnson, PhD – Past Investigator

Premiere Research Inst (Palm Beach Neurology):
Carl Sadowsky, MD
Teresa Villena, MD

Georgetown University Medical Center:
Raymond Scott Turner, MD, PhD
Kathleen Johnson, NP
Brigid Reynolds, NP

Brigham and Women's Hospital:
Reisa A. Sperling, MD
Keith A. Johnson, MD
Gad Marshall, MD

Stanford University:
Jerome Yesavage, MD
Joy L. Taylor, PhD
Barton Lane, MD
Allyson Rosen, PhD – Past Investigator
Jared Tinklenberg, MD – Past Investigator

Banner Sun Health Research Institute:
Marwan N. Sabbagh, MD
Christine M. Belden, PsyD
Sandra A. Jacobson, MD
Sherye A. Sirrel, CCRC

Boston University:
Neil Kowall, MD
Ronald Killiany, PhD
Andrew E. Budson, MD
Alexander Norbash, MD – Past Investigator
Patricia Lynn Johnson, BA – Past Investigator

Howard University:
Thomas O. Obisesan, MD, MPH
Saba Wolday, MSc
Joanne Allard, PhD

Case Western Reserve University:
Alan Lerner, MD
Paula Ogrocki, PhD
Curtis Tatsuoka, PhD
Parianne Fatica, BA, CCRC

University of California, Davis – Sacramento:
Evan Fletcher, PhD
Pauline Maillard, PhD
John Olichney, MD
Charles DeCarli, MD – Past Investigator
Owen Carmichael, PhD – Past Investigator

Neurological Care of CNY:
Smita Kittur, MD – Past Investigator

Parkwood Hospital:
Michael Borrie, MB ChB
T-Y Lee, PhD
Dr Rob Bartha, PhD

University of Wisconsin:
Sterling Johnson, PhD
Sanjay Asthana, MD
Cynthia M. Carlsson, MD, MS

University of California, Irvine - BIC:
Steven G. Potkin, MD
Adrian Preda, MD
Dana Nguyen, PhD

Banner Alzheimer's Institute:
Pierre Tariot, MD
Anna Burke, MD
Ann Marie Milliken, NMD
Nadira Trncic, MD, PhD, CCRC – Past Investigator
Adam Fleisher, MD – Past Investigator
Stephanie Reeder, BA – Past Investigator

Dent Neurologic Institute:
Vernice Bates, MD
Horacio Capote, MD
Michelle Rainka, PharmD, CCRP

Ohio State University:
Douglas W. Scharre, MD
Maria Kataki, MD, PhD
Brendan Kelley, MD

Albany Medical College:
Earl A. Zimmerman, MD
Dzintra Celmins, MD
Alice D. Brown, FNP

Hartford Hospital, Olin Neuropsychiatry Research Center:
Godfrey D. Pearlson, MD
Karen Blank, MD
Karen Anderson, RN

Dartmouth-Hitchcock Medical Center:
Laura A. Flashman, PhD
Marc Seltzer, MD
Mary L. Hynes, RN, MPH
Robert B. Santulli, MD – Past Investigator

Wake Forest University Health Sciences:
Kaycee M. Sink, MD, MAS
Leslie Gordineer
Jeff D. Williamson, MD, MHS – Past Investigator
Pradeep Garg, PhD – Past Investigator
Franklin Watkins, MD – Past Investigator

Rhode Island Hospital:
Brian R. Ott, MD
Geoffrey Tremont, PhD
Lori A. Daiello, Pharm.D, ScM

Butler Hospital:
Stephen Salloway, MD, MS
Paul Malloy, PhD
Stephen Correia, PhD

UC San Francisco:
Howard J. Rosen, MD
Bruce L. Miller, MD
David Perry, MD

Medical University South Carolina:
Jacobo Mintzer, MD, MBA
Kenneth Spicer, MD, PhD
David Bachman, MD

St. Joseph's Health Care:
Elizabeth Finger, MD
Stephen Pasternak, MD
Irina Rachinsky, MD
John Rogers, MD
Andrew Kertesz, MD – Past Investigator
Dick Drost, MD – Past Investigator

Nathan Kline Institute
Nunzio Pomara, MD
Raymundo Hernando, MD
Antero Sarrael, MD

University of Iowa College of Medicine
Susan K. Schultz, MD
Karen Ekstam Smith, RN
Hristina Koleva, MD
Ki Won Nam, MD
Hyungsub Shim, MD– Past Investigator

Cornell University
Norman Relkin, MD, PhD
Gloria Chiang, MD
Michael Lin, MD
Lisa Ravdin, PhD

University of South Florida: USF Health Byrd Alzheimer's Institute
Amanda Smith, MD
Balebail Ashok Raj, MD
Kristin Fargher, MD– Past Investigator

ADNI Participating Institutions

Johns Hopkins University; Washington University, St. Louis; University of California, Los Angeles; University of Pennsylvania; Cleveland Clinic Lou Ruvo Center for Brain Health; Sunnybrook Health Sciences Centre; Parkwood Hospital; University of California, San Diego; University of Kansas; Dent Neurologic Institute; McGill University / Jewish General Hospital Memory Clinic; Rush University Medical Center; Baylor College of Medicine; Duke University Medical Center; Wein Center for Clinical Research; Indiana University; St. Joseph's Health Center – Cognitive Neurology; Banner Alzheimer's Institute; New York University Medical Center; Mayo Clinic, Jacksonville; Mount Sinai School of Medicine; University of Michigan, Ann Arbor; University of British Columbia, Clinic for AD & Related; University of Wisconsin; Oregon Health and Science University; Northwestern University; Boston University; Case Western Reserve University; Emory University; University of Pittsburgh; Brigham and Women's Hospital; University of Alabama, Birmingham; Medical University of South Carolina; University of California, Irvine; Howard University; University of California, Davis; Rhode Island Hospital; Mayo Clinic, Rochester; Nathan Kline Inst. for Psychiatric Rsch; University of Rochester Medical Center; University of California, Irvine (BIC); The Weill Cornell Memory Disorders Program; Georgetown University; University of California, San Francisco; Banner Sun Health Research Institute; Premiere Research Institute; Butler Hospital Memory and Aging Program; Dartmouth Medical Center; Ohio State University; University of Southern California; University of Iowa; Wake Forest University Health Sciences; University of Kentucky; University of South Florida, Tampa; Columbia University; Yale University School of Medicine; University of Texas, Southwestern MC; Stanford / PAIRE; Albany Medical College.

The list is also available online at http://adni.loni.usc.edu/about/centers-cores/study-sites/.